Quaternary Science Reviews 167 (2017) 30–46

Contents lists available at ScienceDirect

Quaternary Science Reviews

journal homepage: www.elsevier.com/locate/quascirev

Cosmogenic exposure age constraints on deglaciation and flow behaviour of a marine-based ice stream in western Scotland, 21–16 ka

David Small [a, *], Sara Benetti [b], Dayton Dove [c], Colin K. Ballantyne [d], Derek Fabel [e], Chris D. Clark [f], Delia M. Gheorghiu [g], Jennifer Newall [a], Sheng Xu [e]

[a] Department of Geographical and Earth Sciences, University of Glasgow, Glasgow G12 8QQ, UK
[b] School of Environmental Sciences, University of Ulster, Coleraine BT52 1SA, UK
[c] British Geological Survey, The Lyell Centre, Edinburgh EH14 4AP, UK
[d] School of Geography and Sustainable Development, University of St Andrews, St Andrews KY16 9AL, UK
[e] SUERC AMS Laboratory, Scottish Universities Environmental Research Centre, East Kilbride G75 0QF, UK
[f] Department of Geography, University of Sheffield, Sheffield S10 2TN, UK
[g] NERC Cosmogenic Isotope Analysis Facility, SUERC, East Kilbride G75 OQF, UK

ARTICLE INFO

Article history:
Received 20 September 2016
Received in revised form
21 April 2017
Accepted 24 April 2017
Available online 6 May 2017

Keywords:
Exposure dating
Marine ice stream
British-Irish ice sheet
Deglaciation

ABSTRACT

Understanding how marine-based ice streams operated during episodes of deglaciation requires geochronological data that constrain both timing of deglaciation and changes in their flow behaviour, such as that from unconstrained ice streaming to topographically restricted flow. We present seventeen new ^{10}Be exposure ages from glacial boulders and bedrock at sites in western Scotland within the area drained by the Hebrides Ice Stream, a marine-based ice stream that drained a large proportion of the former British-Irish Ice Sheet. Exposure ages from Tiree constrain deglaciation of a topographic high within the central zone of the ice stream, from which convergent flowsets were produced during ice streaming. These ages thus constrain thinning of the Hebrides Ice Stream, which, on the basis of supporting information, we infer to represent cessation of ice streaming at 20.6 ± 1.2 ka, 3–4 ka earlier than previously inferred. A period of more topographically restricted flow produced flow indicators superimposed on those relating to full ice stream conditions, and exposure ages from up-stream of these constrain deglaciation to 17.5 ± 1.0 ka. Complete deglaciation of the marine sector of the Hebrides Ice Stream occurred by 17–16 ka at which time the ice margin was located near the present coastline. Exposure ages from the southernmost Outer Hebrides (Mingulay and Barra) indicate deglaciation at 18.9 ± 1.0 and 17.1 ± 1.0 ka respectively, demonstrating that an independent ice cap persisted on the southern Outer Hebrides for 3–4 ka after initial ice stream deglaciation. This suggests that deglaciation of the Hebrides Ice Stream was focused along major submarine troughs. Collectively, our data constrain initial deglaciation and changes in flow regime of the Hebrides Ice Stream, final deglaciation of its marine sector, and deglaciation of the southern portion of the independent Outer Hebrides Ice Cap, providing chronological constraints on future numerical reconstructions of this key sector of the former British-Irish Ice Sheet.

1. Introduction

Ice streams are faster flowing corridors of ice that exert a major control on the mass balance of ice sheets both past and present (Stokes and Clark, 2001; Bennett, 2003; Stokes et al., 2016). They extend into the accumulation zones of ice sheets and, as well as draining large areas, act as conduits to transmit the effects of external perturbations, such as changes in ocean temperature, air temperature or sea-ice distribution, from periphery to interior (Payne et al., 2004; Shepherd et al., 2004; Stokes et al., 2005; Roberts et al., 2010; Favier et al., 2014). Temporal constraints on ice stream evolution therefore provide information on the dynamics of former ice sheets and are vital for empirical reconstructions of past ice sheet deglaciation (e.g. Hughes et al., 2016). In turn these provide data to test the numerical ice sheet models that are fundamental to predicting future sea-level rise

* Corresponding author.
E-mail address: David.Small@glasgow.ac.uk (D. Small).

http://dx.doi.org/10.1016/j.quascirev.2017.04.021

from modern day ice sheet decay in Greenland and Antarctica (e.g. Alley et al., 2005; DeConto and Pollard, 2016).

Studies of extant ice sheets have observed a range of behaviour in ice streams including acceleration, deceleration, stagnation, reactivation, and migration (Retzlaff and Bentley, 1993; Jacobel et al., 1996; Anandakrishnan et al., 2001; Conway et al., 2002; Hulbe and Fahnestock, 2004; Joughin et al., 2004; Catania et al., 2006; Howat et al., 2007). However, given the temporal limitations of modern observations, understanding the longer-term significance of such changes remains challenging. In this context palaeo-ice streams provide a geomorphological record of ice stream evolution from maximum extent to final deglaciation and can be used to place observed changes in context (e.g. Stokes et al., 2009; Winsborrow et al., 2012; Hughes et al., 2014; Stokes et al., 2016). Reconstructions of past ice streams were initially hindered by the scale of the geomorphological evidence they leave behind with suites of landforms delimiting their extent and flow directions extending over large areas (~10^3–10^5 km^2) that are often relatively

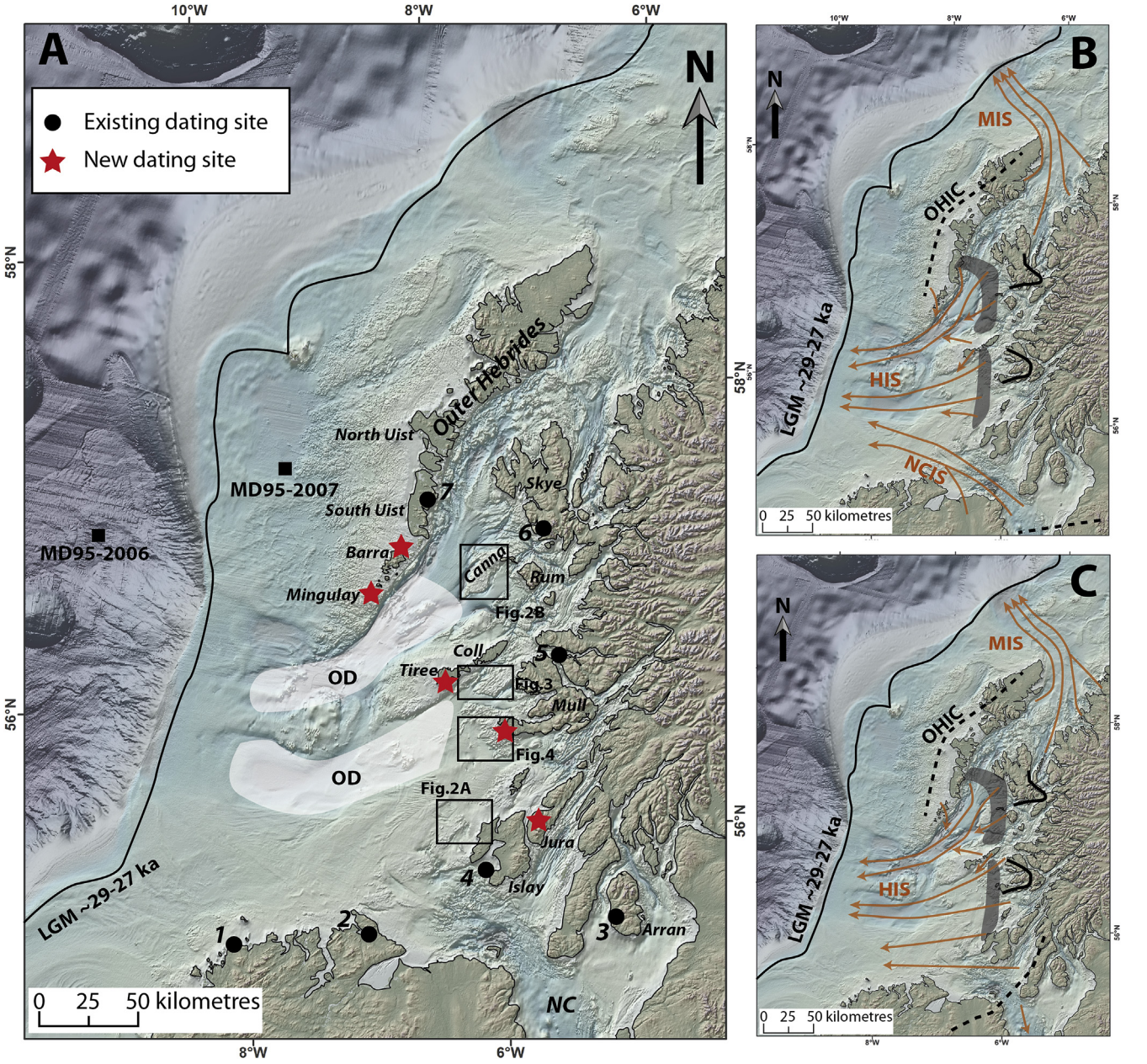

Fig. 1. A. Location map of the Hebrides with regional bathymetry showing the place names mentioned in the text. Black dots indicate existing geochronological data, numbered as in Table 1 (for clarity the existing data from Jura are not numbered). Red stars indicate sites included in this study. White shaded areas are glacial overdeepenings (OD = overdeepening) formerly occupied by the Hebrides Ice Stream. Maximum extent of BIIS as depicted by Bradwell et al. (2008) and adapted by Hiemstra et al. (2013). NC = North Channel. B and C. postulated flowlines of the Hebrides Ice Stream.: (B) during the earlier stage of ice streaming when it was influenced by ice flowing from the North Channel (Finlayson et al., 2014; Hughes et al., 2014); (C) during the later stage of ice streaming when the Hebrides Ice Stream was not influenced by North Channel ice (Dove et al., 2015). The major ice divides relevant to the Hebrides Ice Stream are shown (black dashed lines), including independent ice domes over Skye and Mull (solid black lines). Inferred onset zones of the HIS are shown with black shading in panels B and C. The flowlines of the neighbouring Minch Ice Stream [MIS] (Bradwell et al., 2008) are also shown. HIS = Hebrides Ice Stream, OHIC = Outer Hebrides Ice Cap, NCIS = North Channel Ice Stream. Boxes denote extent of Figs. 2–4. Location of marine cores mentioned in the text are also shown. Bathymetry from EMODNET, onshore hillshaded DEM from Intermap Technologies NEXTMap Britain elevation data. (For interpretation of the references to colour in this figure legend, the reader is referred to the web version of this article.)

inaccessible. Advances in remote sensing have provided a means to reconstruct past ice streams (Clark, 1997). Terrestrial ice streams have been reconstructed from air photos and satellite imagery (e.g. Dyke and Morris, 1988; Stokes and Clark, 2001; De Angelis and Kleman, 2007; Stokes et al., 2009) and, in the marine environment, the increasing availability of high resolution geophysical data, particularly multibeam swath bathymetry, has allowed many former marine-based ice streams to be identified and reconstructed (e.g. Sejrup et al., 2003; Ó'Cofaigh et al., 2005; Ottesen et al., 2005; Andreassen et al., 2008 Bradwell and Stoker, 2015).

Combining suitable data with established geomorphological techniques, such as the 'geomorphological inversion approach' (Clark, 1997; Kleman et al., 2006), has permitted the behaviour of palaeo-ice streams to be investigated (e.g. De Angelis and Kleman, 2007). This approach has enabled researchers to elucidate ice stream dynamics at a variety of spatial scales including holistic overviews of an entire ice sheet (Margold et al., 2015; Stokes et al., 2016; Hughes et al., 2014), studies of ice stream evolution within defined sectors of an ice sheet (Stokes and Clark, 2001; Ottesen et al., 2005; Stokes et al., 2009) and, focused studies of individual ice streams (Sejrup et al., 2003; Dove et al., 2015; Bradwell and Stoker, 2015). Such work has demonstrated the temporal variability of ice streams during deglaciation such as ice stream initiation, termination, acceleration and migration, all of which influence ice sheet mass balance through time (e.g. Stokes et al., 2016). To integrate this improving understanding of ice stream variability into empirical reconstructions that can be used to test numerical ice sheet models (e.g. Hubbard et al., 2009; Patton et al., 2016) requires geochronological data that constrains the behaviour of palaeo-ice streams (e.g. Briner et al., 2009; Roberts et al., 2013; Lane et al., 2014).

In this paper we aim to constrain the timing of deglaciation of a major marine-based ice stream, the Hebrides Ice Stream (HIS), which drained the western part of the former British-Irish Ice Sheet (BIIS). We present seventeen new ^{10}Be cosmogenic exposure ages from the Hebridean islands of western Scotland. By combining this new geochronological control with existing geomorphological reconstructions (Howe et al., 2012; Finlayson et al., 2014; Dove et al., 2015) and chronological evidence (McCabe and Clark, 2003; Clark et al., 2009; Small et al., 2016) previously inferred ice stream evolution can be placed within an absolute chronological framework.

2. Setting

2.1. Regional glaciological setting

The former British-Irish Ice Sheet (BIIS) was drained by fast flowing ice streams across much of its western sector (Ó'Cofaigh and Evans, 2001; Stoker and Bradwell, 2005; Bradwell et al., 2008; Howe et al., 2012; Bradwell and Stoker, 2015; Dove et al., 2015). One of the largest of these was the Hebrides Ice Stream (HIS; cf. Howe et al., 2012), which drained a large portion of the

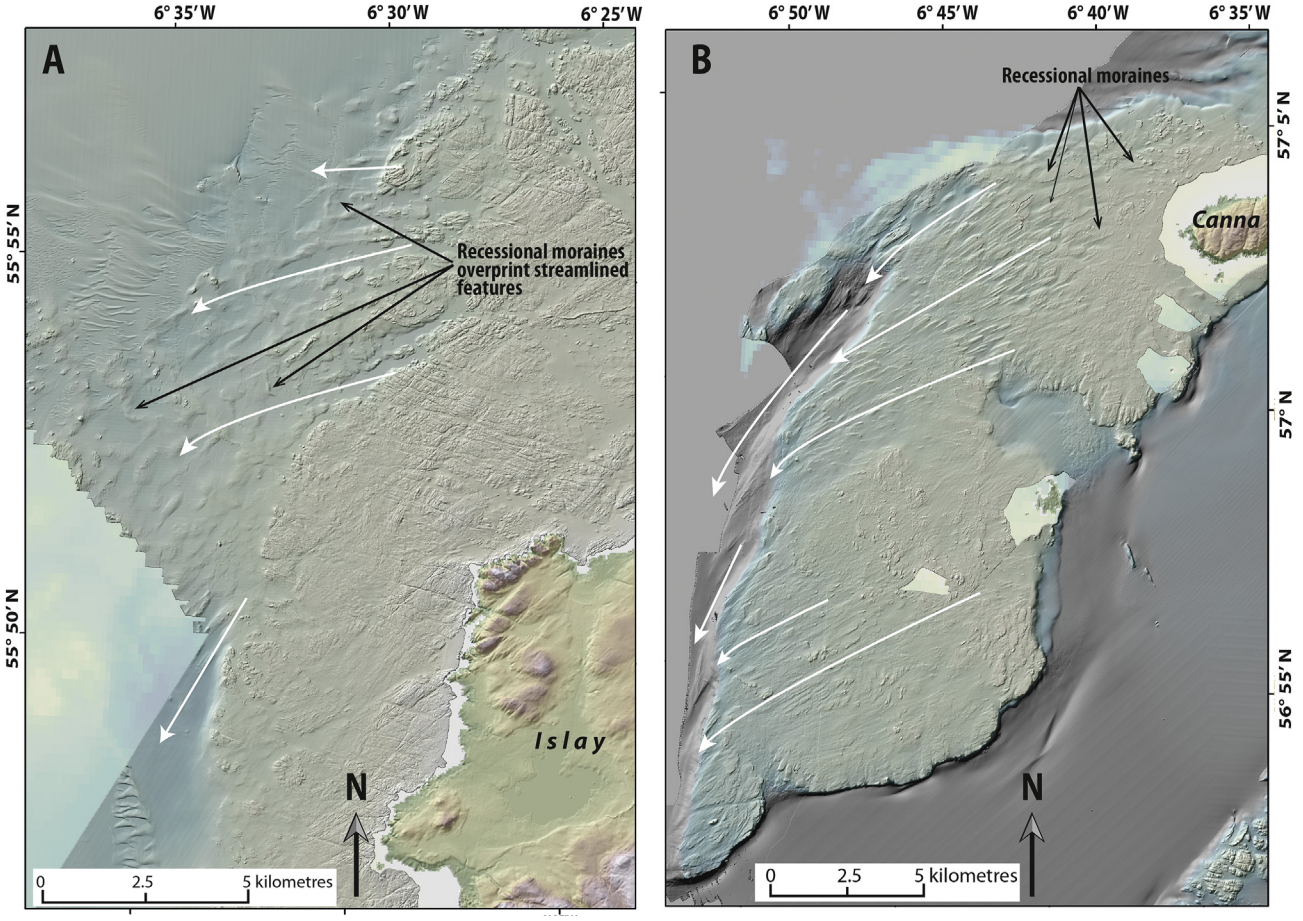

Fig. 2. A. Examples of streamlined landforms west of Islay. These are orientated to the southwest, indicating that at the time of formation flow was little influenced by ice from the North Channel. Suites of recessional moraines can be seen overprinting the streamlined landforms. B. Examples of streamlined landforms southeast of Canna. Flow indicators are orientated towards, and aligned with, the axis of the trough to the west (See Fig. 1). Also highlighted are sinuous ridges, interpreted as possible recessional moraines that overprint streamlining. Bathymetry data provided courtesy of the Maritime & Coastguard Agency's UK Civil Hydrography Programme ©Crown copyright. Terrestrial topography data derived from Intermap Technologies NEXTMap Britain elevation data. Figure adapted from Dove et al. (2015).

western seaboard of Scotland from Skye in the north to Islay in the South (Fig. 1A). High-resolution bathymetric data has allowed the former extent and onset zones of the HIS to be delimited by the distinctive landform assemblages preserved (Fig. 1; Howe et al., 2012; Dove et al., 2015).

At the time of maximum ice-sheet extent the HIS was confluent with the North Channel Ice Stream (NCIS) that drained southwest Scotland and northern Ireland (Fig. 1B: Greenwood and Clark, 2009; Finlayson et al., 2014; Dove et al., 2015) and extended to the Atlantic shelf edge (Bradwell et al., 2008; Dunlop et al., 2010). Subglacial bed forms indicative of HIS flow direction (Fig. 2A), however, apparently relate to a later period of ice streaming when the HIS was only marginally influenced by confluence with the NCIS (Dove et al., 2015). This period of ice streaming (Fig. 1C) is recorded by numerous streamlined landforms up to several kilometres long (Fig. 2B). The orientation of these landforms indicates distinct, convergent flow-sets (Figs. 2B and 3) that define the flow of the HIS. The onset zone (Fig. 1) of ice streaming was seaward of the islands of Rum and Mull as indicated by the transition from bedrock exhibiting limited glacial modification to more streamlined bed forms (Fig. 4; Howe et al., 2012; Dove et al., 2015). Ice flowed SSW onto the outer continental shelf and Dove et al. (2015) suggest that this direction of ice flow was influenced by two pronounced over-deepenings that are ~200 m deeper than the surrounding seafloor and likely formed during previous Quaternary glaciations (Fig. 1A). Additionally, the Outer Hebrides nourished a semi-independent ice cap (Stone and Ballantyne, 2006, Fig. 1), which, along with the platform of Lewisian Gneiss that underlies the Outer Hebrides, probably acted to steer the HIS to the southwest.

Superimposed flow-indicators (Fig. 4) show that following the end of ice stream activity when the HIS was an independent entity with convergent flow and highly elongated sub-glacial bed forms (cf. Stokes and Clark, 2001) flow-directional readjustments occurred. Similarly, terrestrial evidence from other sectors of the BIIS, in the form of flow-sets with divergent orientations and dispersal patterns of erratics, supports a model of evolving ice flow patterns (Greenwood and Clark, 2009; Finlayson et al., 2014) demonstrating ice sheet reorganisation over time, as the ice sheet adjusted its thickness and flow geometric relationship to topography (Hughes et al., 2014). Suites of small recessional moraines overprint the streamlined bed forms indicating numerous still stands or minor oscillations of the ice margin (Figs. 2A and 3). Collectively, these landform assemblages are interpreted as being characteristic of progressively increasing topographic constraints as the ice retreated into confined fjords and basins (Dove et al., 2015).

2.2. Existing geochronology

Geochronological control on the deglaciation of the HIS (Table 1) has been based on three radiocarbon ages from marine shells (Peacock, 2008) and cosmogenic exposure ages from onshore sites

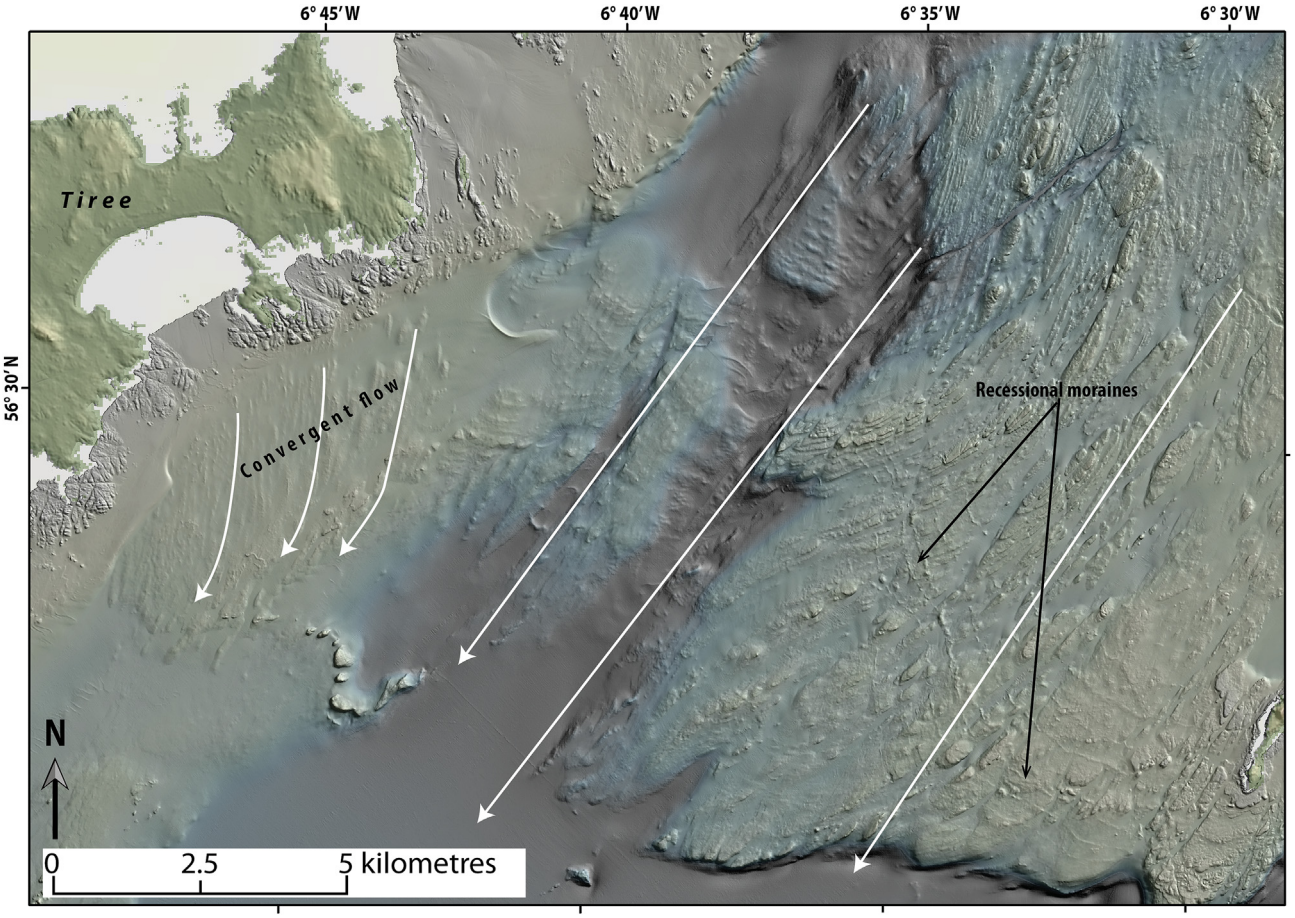

Fig. 3. Flow indicators on the sea floor south of Tiree, interpreted as indicating ice flow southward from the Tiree-Coll platform converging with the Hebrides Ice Stream. Recessional moraines orientated perpendicularly to the streamlined landforms, are clearly visible. Bathymetry data provided courtesy of the Maritime & Coastguard Agency's UK Civil Hydrography Programme ©Crown copyright. Terrestrial topography data derived from Intermap Technologies NEXTMap Britain elevation data. Figure adapted from Dove et al. (2015).

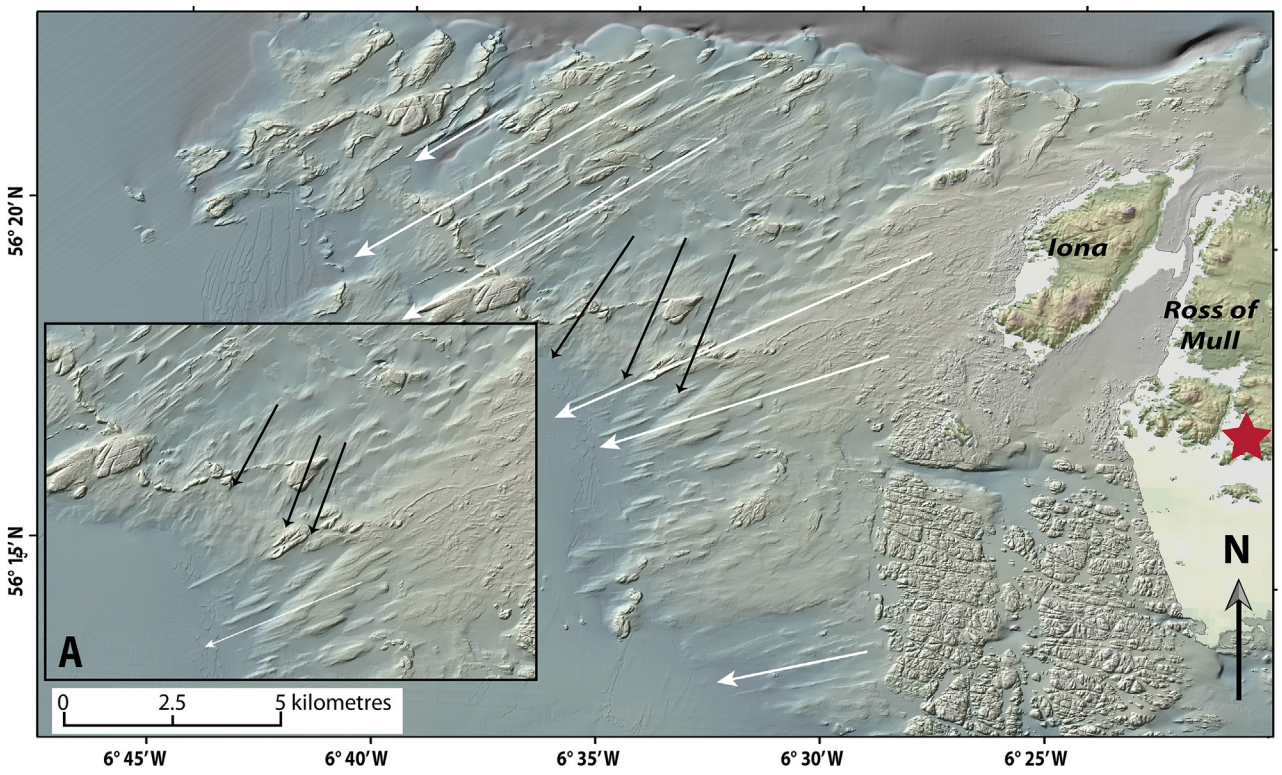

Fig. 4. Superimposed flow indicators west of the Ross of Mull. The dominant flowset (white arrows) is aligned ENE – WSW and is inferred to be related to ice streaming when the HIS had retreated to the mid-shelf (Dove et al., 2015). The later, overprinted flowset (black arrows and inset) is orientated NE-SW and is inferred to be related to later topographically-constrained ice movement. Bathymetry data provided courtesy of the Maritime & Coastguard Agency's UK Civil Hydrography Programme ©Crown copyright. Terrestrial topography data derived from Intermap Technologies NEXTMap Britain elevation data. Figure adapted from Dove et al. (2015).

within the upper reaches of the ice stream. The location of existing geochronological data is shown in Fig. 1A. Initial deglaciation from the shelf edge was underway by ~20 ka as indicated by cosmogenic exposure and radiocarbon ages from the north coast of Ireland (McCabe and Clark, 2003; Ballantyne et al., 2007; Clark et al., 2009; Ballantyne and Ó Cofaigh, 2017). The oldest basal radiocarbon age

Table 1
Published ages referred to in the text. Site numbers refer to Fig. 1. Clusters of exposure ages that yield acceptable x_R^2 values are shown in bold. Underlined radiocarbon ages are the oldest from a site. ^{10}Be Exposure ages calculated using CRONUS online calculator (http://hess.ess.washington.edu; accessed August 19th 2016), Lm scaling and, Loch Lomond Production Rate of 4.00 ± 0.18 atoms g^{-1} yr^{-1} (Fabel et al., 2012). ^{36}Cl exposure ages calculated using CRONUScalc (Marrero et al., 2016). ^{14}C ages calibrated using OxCal 4.2 (Bronk Ramsey, 2013) and Marine14 (Reimer et al., 2013), ΔR = 300 yr.

Reference	Location (site no. Fig. 1)	Sample name	Technique	Age (yr)	Uncert. (yr)
Clark et al. (2009)	N Donegal coast (1)	BF-04-01	^{10}Be	17616	1764
Clark et al. (2009)	N Donegal coast (1)	BF-04-03	^{10}Be	33,057	2940
Clark et al. (2009)	**N Donegal coast (1)**	**BF-04-04**	^{10}Be	**21,469**	**1740**
Clark et al. (2009)	**N Donegal coast (1)**	**BF-04-05**	^{10}Be	**20,931**	**1851**
Clark et al. (2009)	**N Donegal coast (1)**	**BF-04-06**	^{10}Be	**20,954**	**2049**
Clark et al. (2009)	N Donegal coast (1)	BF-04-08	^{10}Be	23,258	2123
Clark et al. (2009)	**N Donegal coast (1)**	**BF-04-09**	^{10}Be	**21,435**	**2186**
Clark et al. (2009)	**N Donegal coast (1)**	**BF-04-10**	^{10}Be	**21,806**	**2179**
McCabe and Clark (2003)	N Donegal coast (2)	AA32315	^{14}C	16,602	178
McCabe and Clark (2003)	N Donegal coast (2)	AA45968	^{14}C	18,676	168
McCabe and Clark (2003)	N Donegal coast (2)	AA45967	^{14}C	17,997	188
McCabe and Clark (2003)	N Donegal coast (2)	AA45966	^{14}C	19,093	496
McCabe and Clark (2003)	N Donegal coast (2)	AA33831	^{14}C	17,913	130
McCabe and Clark (2003)	N Donegal coast (2)	AA33832	^{14}C	20,308	148
Finlayson et al. (2014)	**Arran (3)**	**D1**	**^{10}Be**	**16,088**	**964**
Finlayson et al. (2014)	**Arran (3)**	**D2**	**^{10}Be**	**16,858**	**978**
Peacock (2008)	Islay (4)	SUERC-13122	^{14}C	14,457	163
Peacock (2008)	Islay (4)	SUERC-13123	^{14}C	14,337	149
Peacock (2008)	Islay (4)	SUERC-13124	^{14}C	14,498	166
Baltzer et al. (2010)	W coast of Scotland (5)	UL2853	^{14}C	16,587	311
Small et al. (2016)	**Skye (6)**	**BRI01**	**^{36}Cl**	**18,200**	**1700**
Small et al. (2016)	**Skye (6)**	**BRI02**	**^{36}Cl**	**17,300**	**1600**
Small et al. (2016)	**Skye (6)**	**BRI03**	**^{36}Cl**	**19,400**	**1700**
Small et al. (2016)	**Skye (6)**	**BRI04**	**^{36}Cl**	**15,500**	**1700**
Stone and Ballantyne (2006)	South Uist (7)	BM2	^{10}Be	16,250	878

Table 2
Sample information, chemistry data and measured $^{10}Be/^{9}Be$ ratios for samples reported in this study.

Sample	Location	Latitude	Longitude	Alt. (m)	Thickness (cm)	Shielding Correction [a]	Qtz Mass (g)	Be Spike (μg)[b]	$^{10}Be/^{9}Be$ [c] ($\times10^{-15}$)	Uncert ($\times10^{-15}$)
T7CAR02	Tiree	56.4552	−6.9234	136	1.5	1.000	17.6	232.984[1]	113.00	3.35
T7CAR05	Tiree	56.4546	−6.9227	133	2.4	1.000	21.6	231.320[1]	132.25	3.71
T7CAR07	Tiree	56.4524	−6.9188	111	3.0	1.000	29.3	259.052[1]	162.94	4.69
T7TMC01	Mull	56.2879	−6.3443	42	1.3	0.996	25.1	236.978[1]	117.18	3.26
T7TMC05	Mull	56.2872	−6.3429	57	0.9	1.000	29.9	235.979[1]	147.31	4.16
T7TMC06	Mull	56.2862	−6.3411	46	5.2	0.993	26.6	233.982[1]	126.95	3.71
S1	Jura	55.9176	−6.0509	106	1.0	1.000	18.5	247.303[2]	92.3	3.43
S2	Jura	55.9172	−6.0512	106	6.0	1.000	18.7	247.722[2]	86.5	3.18
S3	Jura	55.9176	−6.0522	92	3.0	1.000	19.9	249.336[2]	82.0	3.57
T7MIN02	Mingulay	56.8210	−7.6306	223	1.5	1.000	30.8	240.173[1]	190.56	4.83
T7MIN03	*Mingulay*	*56.8210*	*−7.6306*	*223*	*2.8*	*1.000*	*37.3*	*240.830[1]*	*260.03*	*6.84*
T7MIN04	Mingulay	56.8200	−7.6317	196	1.7	1.000	37.0	239.845[1]	206.46	4.94
T7MIN06	Mingulay	56.8152	−7.6379	52	1.6	0.999	36.9	240.337[1]	196.14	4.58
T7MIN07	*Mingulay*	*56.8152*	*−7.6379*	*52*	*3.3*	*0.999*	*37.6*	*239.845[1]*	*213.71*	*5.25*
T7SGU02	Barra	57.0526	−7.4493	65	2.0	0.997	22.1	249.012[3]	104.07	2.96
T7SGU03	Barra	57.0527	−7.4496	69	3.0	0.999	21.7	247.399[3]	116.34	3.01
T7SGU04	Barra	57.0535	−7.4511	78	1.0	1.000	21.7	249.521[3]	102.95	2.93

[a] Topographic shielding correction calculated using CRONUS-Earth online calculator (Balco et al., 2008; available at http://hess.ess.washington.edu/math/general/skyline_input.php).
[b] Samples were spiked with ^{9}Be carrier of various concentrations: [1] 1664.2 ± 1.5 μg/g, [2] 299 ± 6 μg/g, [3] 849 ± 12 μg/g.
[c] Relative to NIST_27900 with $^{10}Be/^{9}Be$ taken as 2.79×10^{-11}.

from a mollusc within a marine core proximal to Islay indicates deglaciation of the southern HIS before ~15 ka (Peacock, 2008) and is consistent with ^{10}Be dates from a medial moraine on Jura indicating deglaciation at ~16.8 ka (Ballantyne et al., 2014) and further ^{10}Be dates from western Arran that indicate deglaciation at ~16.5 ka (Finlayson et al., 2014). The timing of deglaciation in the southern sector of the HIS is mirrored in the northern sector where ^{36}Cl exposure ages from the southern coast of Skye show deglaciation by 17.6 ± 1.7 ka (Small et al., 2016).

3. Methods and exposure age calculations

Surface exposure dating often targets moraine boulders to constrain ice margin behaviour and the timing of readvances. Our aim, however, was to constrain the timing of deglaciation at the sample sites described below, located at key terrestrial locations near the onset zones of the HIS to establish when the ice margin backstepped onto to the land surface. We targeted glacially transported and deposited boulders and glacially modified bedrock that exist within small areas, as it is reasonable to assume that samples in close proximity will share a common deglaciation age (Small et al., 2017). With one notable exception (the Scriob na Caillich moraine), our samples were not part of larger glacial landforms and thus do not have any wider morphostratigraphic relationships other than having been deposited by ice during deglaciation. A total of 17 samples were collected, 15 from glacially transported boulders and two from glacially modified bedrock (Table 2). Example sample photographs are shown in Fig. 5. Three boulder samples were collected from each of the following sites: Carnan Mor on Tiree (3 gneiss boulders), the southwest corner of the Ross of Mull (2 granite boulders, 1 schist boulder), the Scriob na Caillich medial moraine on Jura (3 quartzite boulders), Cnoc Mhic-a-Phi and the central valley of Mingulay (3 gneiss boulders, 2 gneiss bedrock samples), and Beinn Sgurabhal on Barra (3 gneiss boulders) (Fig. 1A). The two bedrock samples were collected on Mingulay to create paired boulder-bedrock samples. All samples from any given site were collected within <1 km^2 (Figs. 5–9), and all were collected from crystalline lithologies (i.e. granite, quartzite, gneiss and schist).

Samples were collected from the top surfaces of boulders and from glacially moulded bedrock using hammer and chisel. We selected large upstanding boulders to minimise the potential for disturbance and snow cover. When possible we sampled flat surfaces but recorded strike and dip if necessary using a compass-clinometer. Detailed site descriptions (e.g. geomorphological context, boulder dimensions, evidence of surface weathering) were made for each sample. Sample locations and elevations were recorded using a hand-held GPS with elevations checked against 1:25000 maps. Shielding from surrounding topography was measured and corrected for using the CRONUS-Earth online calculator (Balco et al., 2008; accessed 23/03/2016; http://hess.ess.washington.edu/math/general/skyline_input.php).

Following sample crushing and washing, quartz was separated from the 250–500 μm fraction using standard mineral separation techniques (Kohl and Nishiizumi, 1992) and purified by ultrasonicating in 2% HF/HNO_3 to remove remaining contaminants (mainly feldspars) and meteoric ^{10}Be. The purity of the leached samples was assessed by measuring the aluminium content using flame atomic absorption spectrometry, with bulk Al content considered a proxy for presence of feldspars. Be extraction was carried out at the Cosmogenic Isotope Analysis Facility - Scottish Universities Environmental Research Centre (CIAF - SUERC) and the Cosmogenic Nuclide Laboratory at the University of Glasgow, using procedures based on Child et al. (2000). The $^{10}Be/^{9}Be$ ratios were measured on the 5 MW accelerator mass spectrometer (AMS) at SUERC (Xu et al., 2010). Locational and analytical details for all 17 samples are given in Table 2.

We present ^{10}Be exposure ages calculated using the CRONUS-Earth calculator (Developmental version; Wrapper script 2.3, Main calculator 2.1, constants 2.2.1, muons 1.1; http://hess.ess.washington.edu/math/al_be_v22/al_be_calibrate_v22.php; accessed 18/07/2016; Balco et al., 2008) and the CRONUScalc calculator (http://web1.ittc.ku.edu:8888/2.0/html; accessed 02/06/2016; Marrero et al., 2016). Ages calculated in the CRONUS-Earth calculator (Balco et al., 2008) are calibrated using a local production rate as this reduces scaling uncertainties and can improve agreement with other geochronological techniques (Balco et al., 2009; Fenton et al., 2011; Goehring et al., 2012; Kaplan et al., 2011; Putnam et al., 2010; Young et al., 2013). Two independently calibrated local production rates are available from the British Isles, the Loch Lomond production rate (LLPR) (Fabel et al., 2012) and the Glen Roy production rate (GRPR) (Small and Fabel, 2015). These production rates agree within uncertainties (4.02 ± 0.18 and 4.35 ± 0.21 atoms g^{-1} a^{-1} respectively). However, the LLPR is

derived from direct age control provided by limiting radiocarbon ages (MacLeod et al., 2011), whereas the GRPR is based on assumed ages of tephra within a varve chronology (MacLeod et al., 2015), so here we employ the more securely calibrated LLPR. The CRONUScalc calculator (Marrero et al., 2016) uses a reference production rate that is dependent on the choice of scaling factor used (Borchers et al., 2016; Marrero et al., 2016). For the Lm scaling scheme this reference production rate is 4.00 atoms g^{-1} a^{-1}. The CRONUScalc calculator also allows users to calculate exposure ages using the Lifton-Sato-Dunai scaling scheme (SA) (Lifton et al., 2014) with a reference production rate of 3.92 atoms g^{-1} a^{-1}.

Overall our exposure age results are not sensitive to choice of calculator with CRONUScalc producing ages that differ by <2% (Lm) and <3.5% (SA). Exposure ages calculated using all three approaches are shown in Table 3. For ease of discussion and comparison with previously published work we focus further discussion on the ages calculated using the CRONUS-Earth calculator using the LLPR, scaled with the time-dependent Lm scaling (Lal, 1991; Stone, 2000; Balco et al., 2008) and assuming an erosion rate of 1 mm ka^{-1}. Assuming erosion rates of 2 mm ka^{-1} and 0 mm ka^{-1} makes our ages c. 2% older and c. 1% younger respectively and does not alter our interpretations. Additionally, erosion rates on glaciated crystalline rocks are generally quite low at < 2 mm ka^{-1} (Andre, 2002). Uncertainties cited below are full (external) uncertainties.

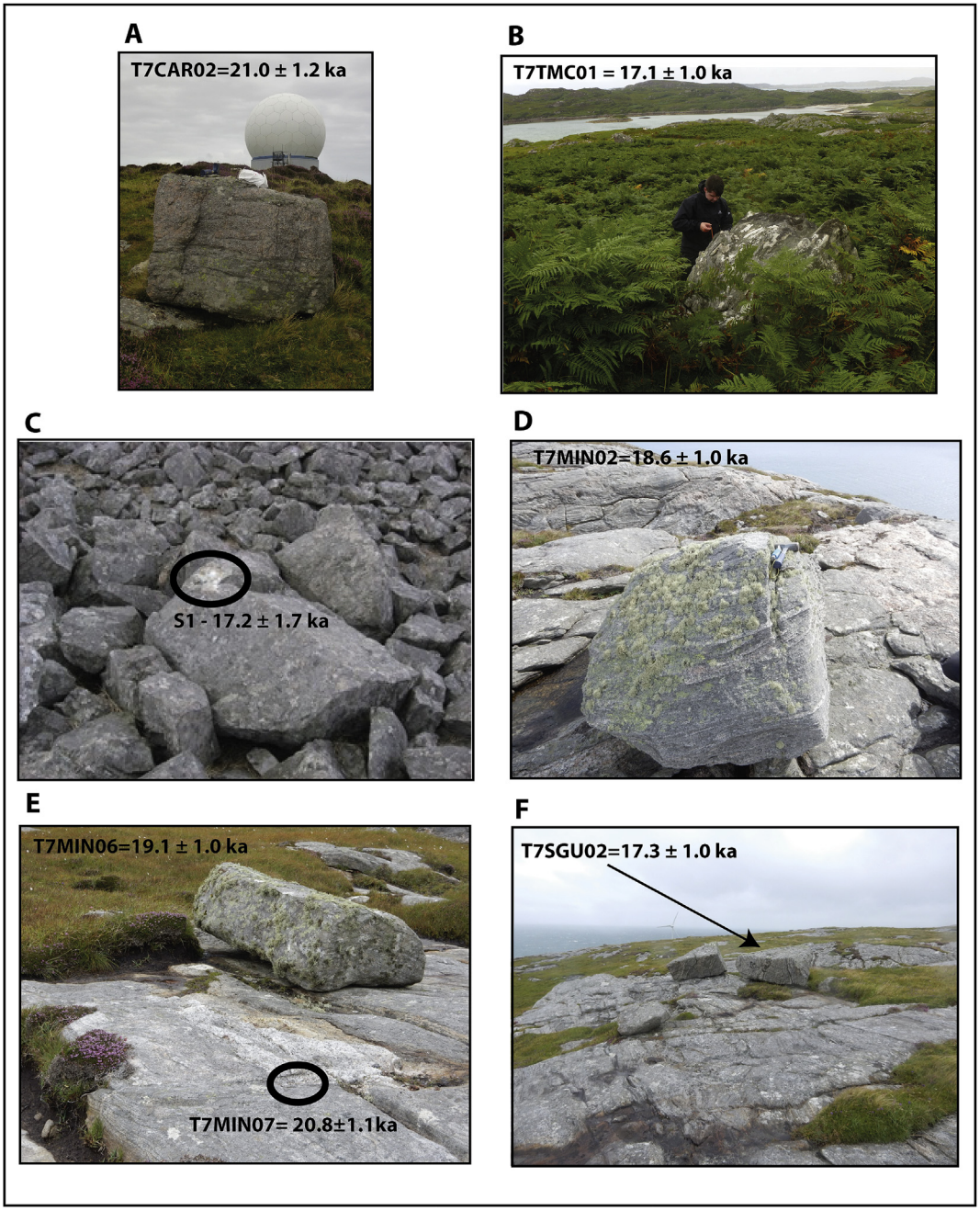

Fig. 5. Examples of sampling sites. A. Boulder (sample T7CAR02) on the summit of Carnan Mór, Tiree, B. Schist erratic (T7TMC01) on the Ross of Mull. C. Boulder (S1) on the Scriob na Caillich medial moraine, Jura. D. Boulder (T7MIN02) on the summit of Cnoc-Mhic a Phi, Mingulay. E. Bedrock-boulder paired samples (T7MIN06 and 07) from the central valley, Mingulay. F. Boulder (T7SGU02) on the summit of Beinn Sgurabhal, Barra.

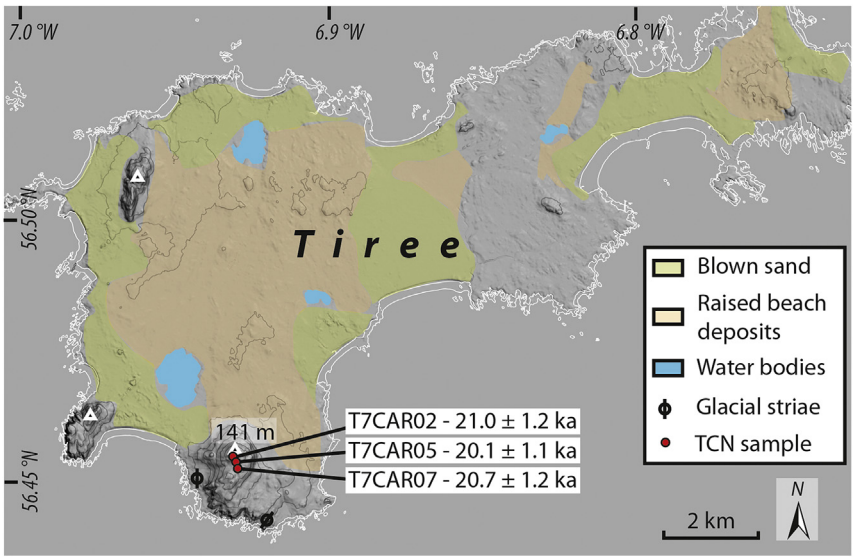

Fig. 6. Location map of Tiree showing areas of raised beach interpreted as a strandflat (Dawson, 1994) that is locally covered by wind blown sand (machair). Major bedrock areas are uncoloured (minor outcrops not shown for clarity). Striae are from British Geological Survey 1:50000 maps. The three Lewisian gneiss hills are located in the west of the island, Carnan Mór (141 m), is the location of the TCN samples (T7CAR02, T7CAR05, T7CAR07). DEM derived from Intermap Technologies NEXTMap Britain elevation data.

4. Results

As noted above, sample sites were selected to constrain the timing of deglaciation of the HIS at key sites adjacent to the onset zones of the HIS. (Figs. 1 and 6–9). In combination with previously published geomorphological evidence, the exposure ages from these sites can provide geochronological data that constrain the timing of deglaciation and changes in the flow behaviour of the HIS. The 17 new exposure ages are summarised in Table 3 and Fig. 10, along with previously published (but recalibrated) ages from the Scriob na Caillich medial moraine (Ballantyne et al., 2014). The ages span the interval 21.5 ± 1.2 ka to 12.3 ± 1.4 ka and generally show reasonable agreement for individual sites. The sites are discussed from youngest to oldest; firstly the Inner Hebrides sites, and then the Outer Hebrides sites.

4.1. Inner hebrides

The Inner Hebrides extend from Skye in the north to Islay in the south, a distance of ~230 km (Fig. 1). Previous suggestions that the last ice sheet terminated on Islay (Synge and Stephens, 1966; Sissons, 1981; Dawson, 1982) are inconsistent with offshore landform and stratigraphic evidence demonstrating that the BIIS terminated on the outer Atlantic Shelf (Knutz et al., 2001; Bradwell et al., 2008; Scourse et al., 2009; Dunlop et al., 2010). It follows that ice flowing from mainland Scotland overran all of the Inner Hebrides (cf. Fabel et al., 2012) except where locally nourished ice domes on Skye and Mull deflected advancing mainland ice (Fig. 1;

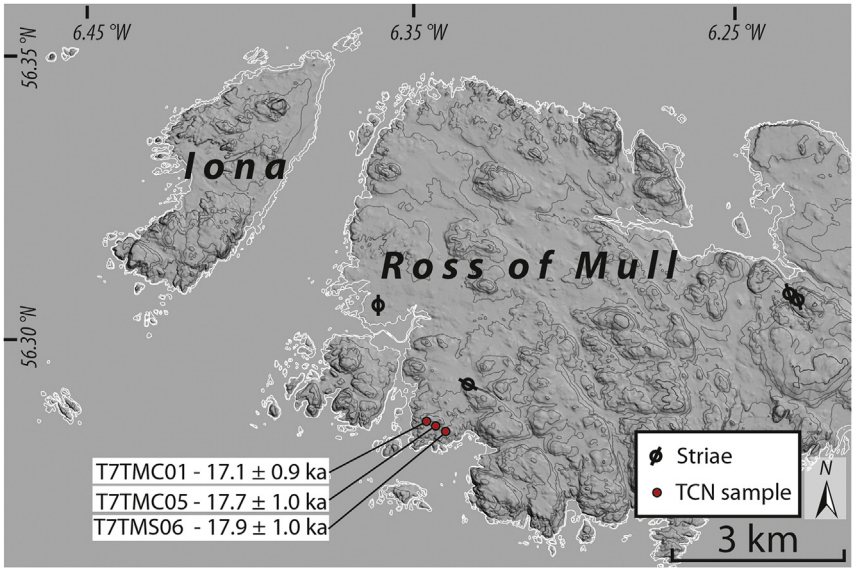

Fig. 7. Location map of the Ross of Mull. Striae are adapted from the BGS 1:50000 map but note the general lack of glacial landforms. Locations of TCN samples T7TMC01, T7TMC05 and T7TMC06 are shown along with their exposure ages. DEM derived from Intermap Technologies NEXTMap Britain elevation data.

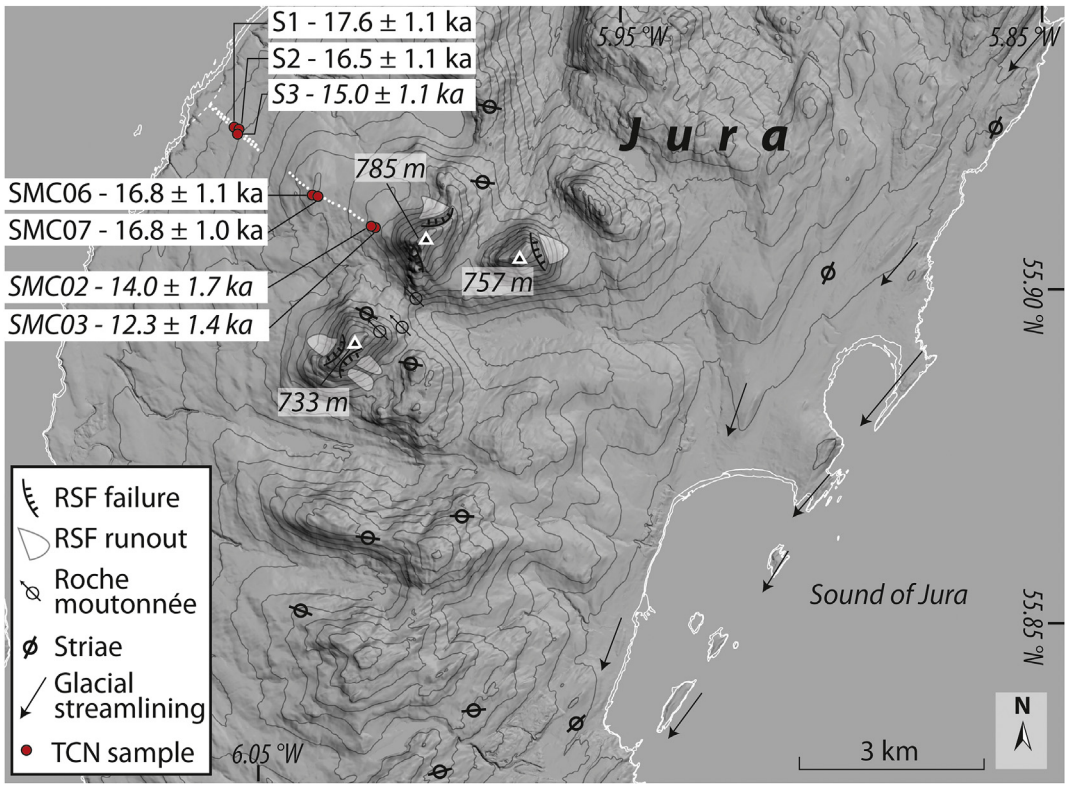

Fig. 8. Location map of Jura. Rock slope failures (RSFs) and their associated runout debris are from Ballantyne et al. (2014). Roches moutonnées are from Ballantyne (1999) with glacial striae from British Geological Survey 1:50000 maps. The locations of the TCN samples from this study (S1-S3) and those presented by Ballantyne et al. (2014) (SMC02,3,6 and 7) are shown with their exposure ages. DEM derived from Intermap Technologies NEXTMap Britain elevation data.

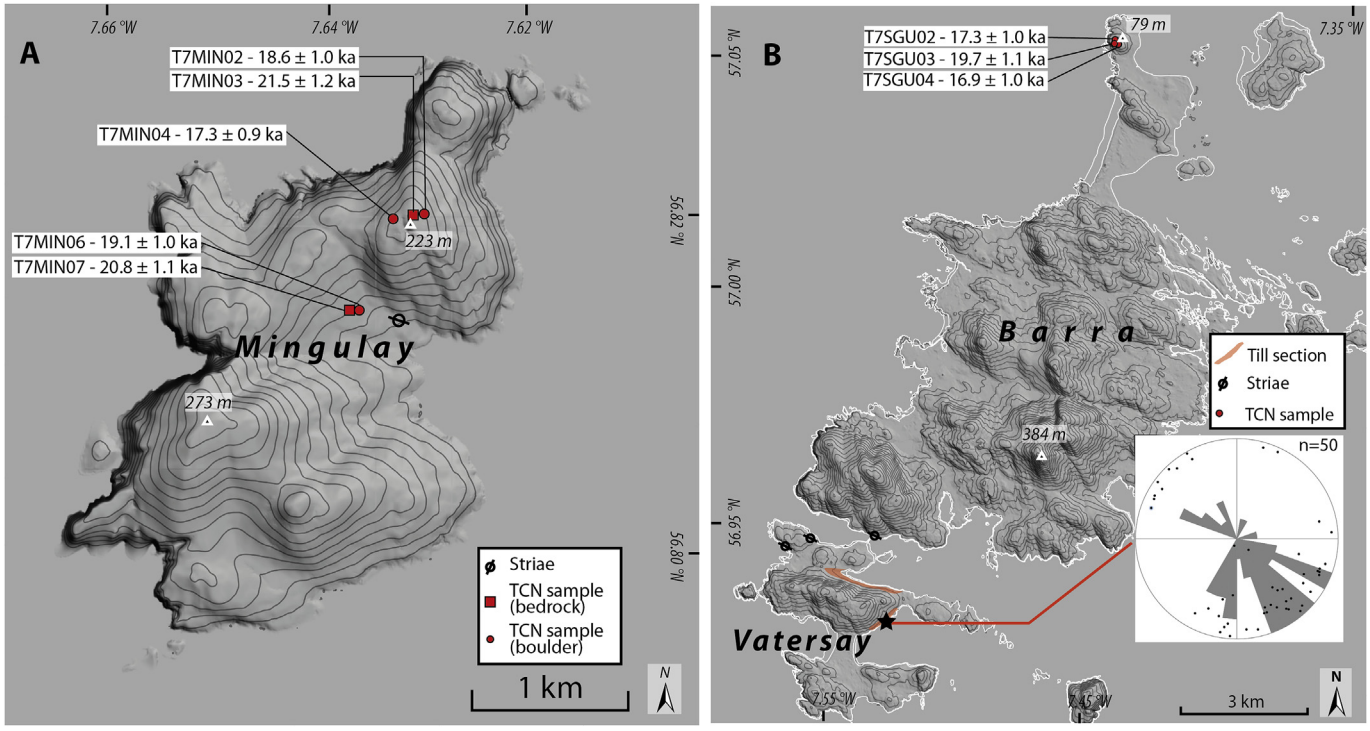

Fig. 9. A. The island of Mingulay, showing locations of bedrock samples (red squares; T7MIN02 and T7MIN07), boulder samples (red circles; T7MIN01, T7MIN04 T7MIN06) and their associated exposure ages. B. The island of Barra showing locations of sampled boulders (T7SGU02-04) and associated exposure ages. Till sections are shown in red, and the inset depicts a rose diagram representing till clast fabric that indicates southwesterly flow through the gap between Barra and Vatersay. This is in agreement with the orientation of observed glacial striae (cf. Peacock, 1984). DEM derived from Intermap Technologies NEXTMap Britain elevation data. (For interpretation of the references to colour in this figure legend, the reader is referred to the web version of this article.)

Table 3
^{10}Be concentrations and calculated exposure ages and uncertainties for all sample reported here. Analytical uncertainties shown in parentheses. Bedrock samples in italics. Also shown (starred) are concentrations and recalculated exposure ages for four samples originally reported in Ballantyne et al. (2014).

Sample	Location	Be conc.	Uncert.	CRONUS-Earth (Lm)[a]		CRONUScalc (Lm)[b]		CRONUScalc (SA)[b]	
				Age	Uncert.	Age	Uncert.	Age	Uncert.
T7CAR02	Tiree	97,776	3206	21.0	1.2 (0.7)	20.7	1.8 (0.7)	20.3	1.7 (0.7)
T7CAR05	Tiree	92,959	2838	20.1	1.1 (0.6)	19.9	1.7 (0.6)	19.6	1.6 (0.6)
T7CAR07	Tiree	93,057	3017	20.7	1.2 (0.7)	20.5	1.7 (0.7)	20.1	1.7 (0.6)
T7TMC01	Mull	72,539	2243	17.1	1.0 (0.5)	17.0	1.4 (0.5)	16.6	1.4 (0.5)
T7TMC05	Mull	76,348	2310	17.7	1.0 (0.5)	17.5	1.5 (0.5)	17.1	1.4 (0.5)
T7TMC06	Mull	73,209	2330	17.9	1.0 (0.6)	17.7	1.5 (0.6)	17.3	1.5 (0.5)
S1	Jura	79,876	3682	17.6	1.2 (0.8)	17.5	1.6 (0.8)	17.2	1.7 (0.8)
S2	Jura	72,019	3454	16.5	1.1 (0.8)	16.4	1.5 (0.8)	16.1	1.4 (0.8)
S3	Jura	66,166	3544	15.0	1.1 (0.8)	14.9	1.4 (0.8)	14.7	1.4 (0.8)
SMC-02*	Jura	80,594	8846	14.0	1.7 (1.6)	13.9	1.9 (1.5)	13.9	1.9 (0.6)
SMC-03*	Jura	70,486	7288	12.3	1.4 (1.3)	12.3	1.6 (1.3)	12.2	1.6 (1.2)
SMC-06*	Jura	95,643	4334	16.8	1.1 (0.8)	16.7	1.5 (0.8)	16.6	1.5 (0.8)
SMC-07*	Jura	94,685	3698	16.8	1.0 (0.7)	16.6	1.5 (0.7)	16.6	1.5 (0.6)
T7MIN02	Mingulay	97,356	2709	18.6	1.0 (0.5)	18.5	1.5 (0.5)	18.3	1.5 (0.5)
T7MIN03	*Mingulay*	*110,712*	*3114*	*21.5*	*1.2 (0.6)*	*21.2*	*1.8 (0.6)*	*21.0*	*1.7 (0.6)*
T7MIN04	Mingulay	87,779	2308	17.3	0.9 (0.5)	17.2	1.4 (0.5)	17.0	1.3 (0.5)
T7MIN06	Mingulay	83,679	2164	19.1	1.0 (0.5)	18.9	1.6 (0.5)	18.5	1.5 (0.5)
T7MIN07	*Mingulay*	*89,493*	*2399*	*20.8*	*1.1 (0.6)*	*20.5*	*1.7 (0.6)*	*20.0*	*1.6 (0.5)*
T7SGU02	Barra	75,754	2578	17.3	1.0 (0.6)	17.2	1.5 (0.6)	16.7	1.4 (0.6)
T7SGU03	Barra	85,853	2670	19.7	1.1 (0.6)	19.5	1.6 (0.6)	19.0	1.6 (0.6)
T7SGU04	Barra	76,155	2600	16.9	1.0 (0.6)	16.8	1.4 (0.6)	16.4	1.4 (0.6)

*Previously reported in Ballantyne et al. (2014).
[a] Calculated using CRONUS calculator; Wrapper script 2.3, Main calculator 2.1, Constants 2.3, Muons 1.1 (Balco et al., 2008). See text for details of local production rates. Ages assume 1 mm ka^{-1} erosion, no inheritance, and density of 2.65 g cm^{-3}. Analytical uncertainties reported in parentheses.
[b] Calculated using CRONUScalc v.1 online exposure age calculator. Production rates described in Borchers et al. (2016).

Harker, 1901; Bailey, 1924; Ballantyne et al., 1998; Ballantyne, 1999).

4.1.1. Tiree

The island of Tiree (Fig. 6) is the westernmost of the Inner Hebrides and is composed entirely of Lewisian Gneiss. Submarine evidence of flow directions presented by Dove et al. (2015) and terrestrial evidence from the nearby Treshnish Isles (Dawson, 1994) indicate southwesterly flow of ice across the island. The topography of Tiree itself is dominated by a planated surface, interpreted as strandflat (Fig. 6), that is locally covered by machair (dune grassland unique to Western Scotland and north-west Ireland) (Dawson, 1994). Three isolated hills protrude above this surface, the highest of these being Carnan Mór (141 m). The summit area of Carnan Mór is littered with abundant large glacially-emplaced boulders. Three samples (T7CAR02, T7CAR05, T7CAR07) collected from prominent boulders have exposure ages of 20.1 ± 1.1 ka to 21.0 ± 1.2 ka that agree within their analytical uncertainties (Fig. 10). These ages have a reduced Chi-square (χ^2_R) value of 0.45 indicating that they are not significantly affected by geological uncertainty (Balco, 2011). The arithmetic mean age and uncertainty is 20.6 ± 1.2 ka (full uncertainty) which we consider a good representation of the true exposure age. For comparison the uncertainty weighted mean (UWM) is 20.6 ± 1.1 ka.

4.1.2. Ross of Mull

The Ross of Mull site (Fig. 7) is located at the southwesternmost extremity of the Isle of Mull, ~40 km SE of Tiree, and is composed of granite. During the Last Glacial Maximum (LGM), central. The Ross of Mull is characterised by exposed granitic bedrock exhibiting some ice moulded surfaces but no clear indicators of flow direction were observed. The general lack of streamlined features is also evident in the offshore bathymetric record, where bedrock exposed south of Iona is devoid of streamlining (Dove et al., 2015, Fig. 4). Striations recording both E–W and N–S ice flow (Fig. 7) are recorded on published geological maps, broadly consistent with a transition from ice streaming to a later period of topographically controlled ice flow recorded by the superimposed flow indicators evident in the offshore bathymetric record (Dove et al., 2015, Fig. 4). Glacially-deposited granite boulders are abundant across the Ross of Mull, but only a single psammite erratic was observed. Many of the granite boulders are sub-rounded and faceted, indicative of sub-glacial transport, and boulders. Perched on glacially moulded bedrock are common. We sampled both the single psammite erratic (T7TMC01) and two granite boulders (T7TMC05, T7TMC06), all located in the southwest corner of the area (Fig. 7). These samples produced exposure ages 17.1 ± 1.0 to 17.9 ± 1.5 ka that also agree within their analytical uncertainties (Fig. 5). They have a $\chi^2_R = 0.41$, consistent with sampling within a single age population, and an arithmetic mean age of 17.5 ± 1.0 ka that we accept as the best estimate for the timing of deglaciation (UWM = 17.5 ± −0.9 ka).

4.1.3. Scriob na Caillich moraine – Jura

Our sampling site on the Isle of Jura lies ~45 km SSE of that on the Ross of Mull, on the Scriob na Caillich medial moraine, a conspicuous linear belt of quartzite boulders sourced from a rockslide onto the surface of the thinning ice sheet (Dawson, 1979; Ballantyne et al., 2014). Numerous striae and roches moutonnées indicate former westward ice flow across Jura (Ballantyne, 1999; Finlayson et al., 2014), implying that during the last ice-sheet maximum ice moving westward across the island fed the HIS. Streamlined landforms on the east coast of Jura (Dove et al., 2015, Fig. 8) indicate SSW flow of ice within the Sound of Jura, but the WNW alignment of the Scriob na Caillich moraine indicates that a westerly flow of ice was maintained across western Jura during ice-sheet thinning. Ballantyne et al. (2014) obtained four ^{10}Be exposure ages (SMC-02, -03, -06 and -07) for samples from boulders on the moraine (Table 3) to constrain the timing of deglaciation. Two of these (SMC-06 and -07) produced identical ages (16.8 ± 1.1 ka and 16.8 ± 1.0 ka) indicating the timing of deglaciation. The much younger ages (14.0 ± 1.7 ka and 12.3 ± 1.4 ka) obtained for the two samples from near the upslope terminus of the moraine were attributed to former burial of this section of the boulder spread by

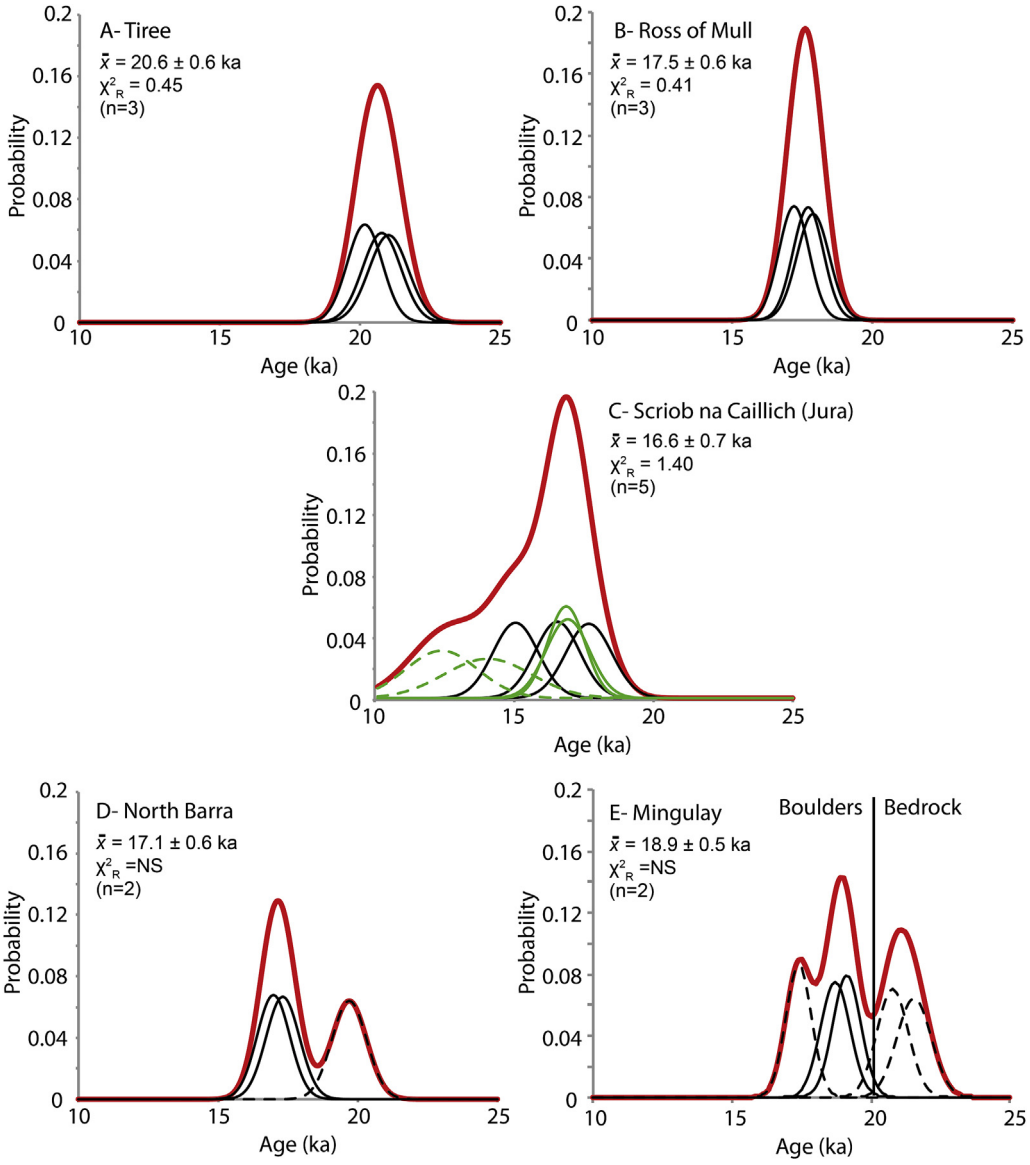

Fig. 10. Summed normal kernel density estimates of exposure ages and their analytical uncertainties (red line), and kernel density estimates of individual exposure ages and their analytical uncertainties (black lines); ages from Ballantyne et al. (2014) are shown in green. All ages were calculated using the CRONUS-Earth online calculator and the LLPR production rate. Ages rejected as representing probable outliers are shown as dashed lines. (For interpretation of the references to colour in this figure legend, the reader is referred to the web version of this article.)

former sediment or peat cover, and rejected as outliers. It is notable that the mean exposure ages obtained by Ballantyne et al. (2014) for five postglacial rockslide runout deposits at the foot of the mountains of Jura (Fig. 8) all post-date their assumed deglaciation age of ~16.8 ka, but that two rockslide ages exceed the rejected younger ages, confirming that the latter are unrepresentative. Our three new exposure ages (S1–S3) from the same medial moraine (Fig. 8) have exposure ages of 17.6 ± 1.2 ka, 16.5 ± 1.1 ka and 15.0 ± 1.1 ka. Tested using analytical uncertainties, all are statistically indistinguishable from the two ages of ~16.8 ka obtained by Ballantyne et al. (2014). Collectively all five ages yield an arithmetic mean exposure age of 16.6 ± 1.1 ka (UWM = 16.6 ± 0.8 ka) with $\chi^2_R = 1.40$, consistent with sampling from a single age population with four degrees of freedom (Bevington and Robinson, 2003).

4.2. Outer hebrides

The evidence provided by striae, roches moutonnées and erratic transport strongly indicates that the Outer Hebrides supported an independent ice cap or ice dome that persisted throughout the build-up and retreat of the last ice sheet, and that the former ice divide of the Outer Hebrides Ice Cap was located over the mountains of Harris and Lewis in the north near the west coast of the Uists in the south (Flinn, 1978; Von Weymarn, 1979; Peacock, 1981, 1984, 1991; Stone and Ballantyne, 2006). The Outer Hebrides Ice Cap deflected ice movement from the NW Highlands and Inner Hebrides both northwards to feed the MIS (Bradwell and Stoker, 2015) and southwards to feed the HIS (Howe et al., 2012; Dove et al., 2015). As the northern margin of the HIS has been depicted as crossing or lying close to the southernmost part of the Outer Hebrides (Fig. 1A and B), we obtained samples from the southern islands of Mingulay and Barra to determine the timing of

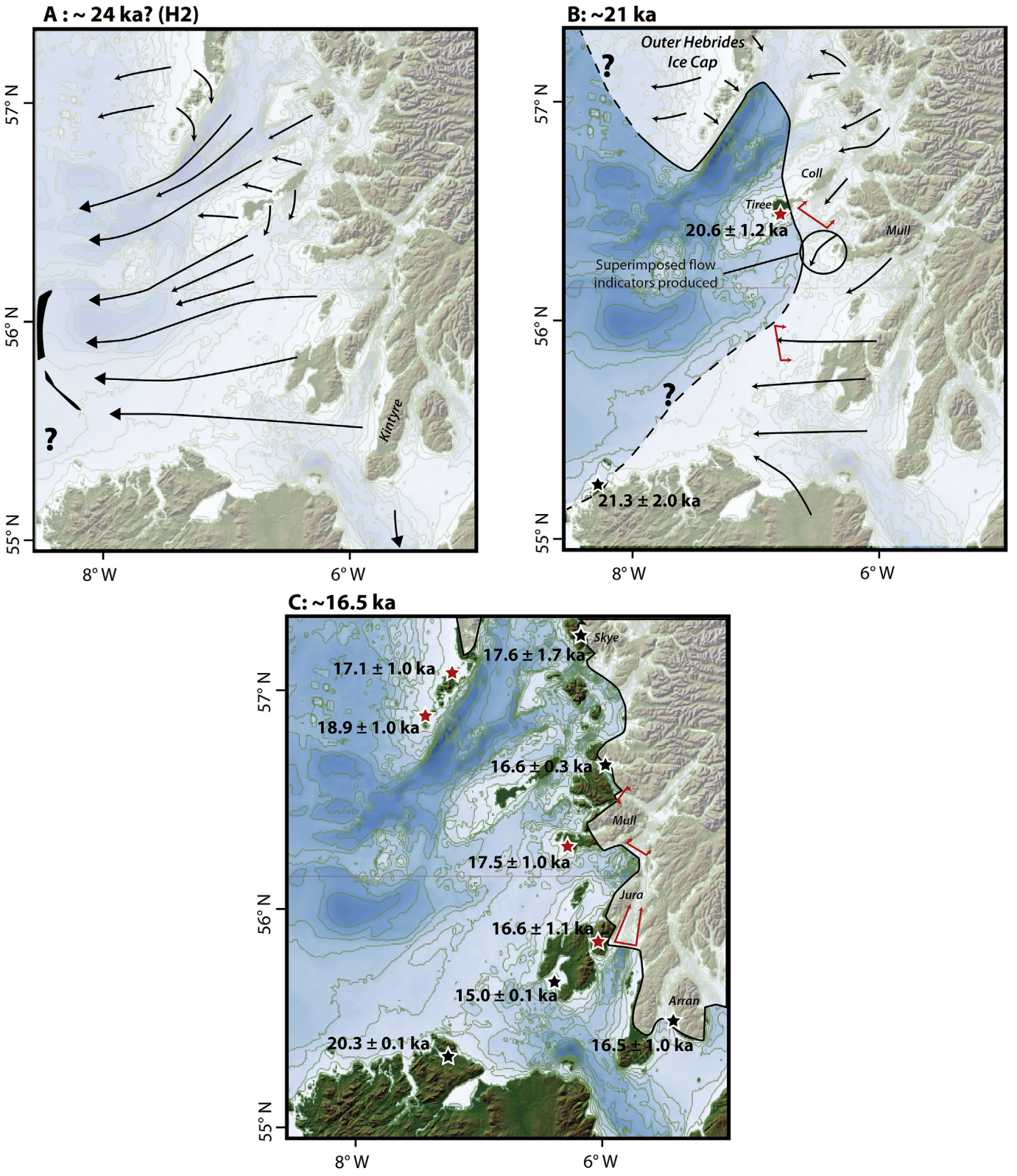

Fig. 11. Schematic deglaciation and flow evolution of the Hebrides Ice Stream. Black arrows indicate flow directions, partly adapted from Dove et al. (2015) and Finlayson et al. (2014). Red arrows indicated inferred direction of ice margin retreat based on the location of recessional moraines (Dove et al., 2015, Fig. 2A and 3). Locations of deglaciation ages presented in this study are shown by red stars, previously-published data (Table 1) by black stars. A. Configuration during the later period of ice streaming (Fig. 1C) as inferred from streamlined landforms (Howe et al., 2012; Dove et al., 2015). The location of large offshore moraines deposited by Scottish ice (Dunlop et al., 2010) is shown in black; the alignment of these moraines suggests that these were produced during this later period of ice streaming following weakening of the North Channel Ice Stream. We very tentatively suggest this configuration may have occurred around the time of, and perhaps in response to, Heinrich Event 2 (H2) at ~24 ka. B.By 21–20 ka the ice margin has retreated to NW Ireland (Clark et al., 2009) and exposed Tiree. We infer that rapid deglaciation was focused in the major offshore troughs adjacent to the Tiree-Coll platform with northward extension of a marine embayment separating ice from the Scottish mainland from the Outer Hebrides Ice Cap. Persistence of the latter at this time is demonstrated by the much

deglaciation on these islands.

4.2.1. Mingulay

Mingulay lies ~60 km NW of Tiree (Fig. 1) and consists of a broad valley separating hills 223 m and 273 m in altitude (Fig. 9A). It is composed entirely of Lewisian Gneiss. The higher ground exhibits subtle evidence of glacial modification (i.e. ice moulded surfaces), but glacially deposited gneiss boulders are common. The central valley contains ice-scoured bedrock, and near sea level striae are aligned WNW–ESE. Five samples were collected: paired bedrock and boulder samples (T7MIN-02 and -03) from the summit of the lower hill, Cnoc Mhic-a-Phi (223 m),; a boulder sample (T7MIN-04) from 196 m west of the same summit; and a further bedrock-boulder pair (T7MIN-06 and -07) from 52 m in the central valley (Fig. 9A).

The five exposure ages obtained for the Mingulay samples span the interval 17.2 ± 0.9 to 21.5 ± 1.2 ka, and collectively yield χ^2_R = 9.83, indicating that they are very unlikely to represent a single age population. The two bedrock samples (T7MIN-03 and T7MIN-06) produced greater apparent ages (21.5 ± 1.2 ka and 20.8 ± 1.1 ka respectively) that the associated boulder samples (18.6 ± 1.0 ka and 19.1 ± 1.0 ka respectively; Fig. 10), suggesting that they are affected by nuclide inheritance due to previous exposure and insufficient rock removal (cf. Heyman et al., 2011). The ages obtained for the three boulder samples yield χ^2_R = 3.58, also indicating that it is unlikely that they are drawn from the same age population. However, two of these samples, T7MIN-02 (18.6 ± 1.0 ka) and T7MIN-06 (19.1 ± 1.0 ka) agree within their analytical uncertainties, and we consider the mean age of these samples, 18.9 ± 1.0 ka (UWM = 18.9 ± 1.0 ka), as the best estimate of deglaciation age on Mingulay, whilst acknowledging that other interpretations of our age data (particularly later deglaciation, as indicated by the age of 17.3 ± 0.9 ka obtained for sample T7MIN-04) cannot be definitively ruled out.

4.2.2. Barra

Three samples (T7SGU-02, -03 and −04) were obtained from glacially-deposited gneiss boulders near the 79 m summit of Beinn Sgurabhal, the northernmost hill on Barra, ~27 km N of Mingulay. Clast fabric analysis of a till exposure on the adjacent island of Vatersay (Fig. 9B) indicates former ice movement approximately NW–SE, consistent with the orientation of nearby striae and wider evidence suggesting that the ice divide of the Outer Hebrides Ice Cap lay west of the southern Outer Hebrides (Peacock, 1981, 1984, 1991; Stone and Ballantyne, 2006). Glacially deposited boulders are common on Barra and bedrock exhibits abundant signs of glacial abrasion and ice moulding, particularly on lower ground and in the gap between Barra and Vatersay.

The three Barra TCN samples produced apparent exposure ages 16.9 ± 1.0 to 19.7 ± 1.1 ka, which yield χ^2_R = 5.85, indicating that the ages are inconsistent with sampling from a single age population and are affected by geological uncertainty. However, the exposure ages obtained for samples T7SGU-02 and T7SGU-04 (17.3 ± 1.0 ka and 16.9 ± 1.0 ka respectively) are consistent, suggesting that the significantly greater age obtained for the third sample (T7SGU-03; 19.7 ± 1.1 ka) is compromised by nuclide inheritance due to prior exposure. The mean exposure age of 17.1 ± 1.0 ka (UWM = 17.1 ± 1.0 ka) for samples T7SGU-02 and T7SGU-04 is therefore accepted as approximating the timing of deglaciation on north Barra.

5. Discussion

5.1. Timing of deglaciation in the Inner Hebrides

The exposure ages presented here constrain the timing of deglaciation in the Inner Hebrides of Scotland and are discussed from oldest to youngest. The inferred timing of deglaciation of Carnan Mór (141 m) on Tiree (20.6 ± 1.2 ka) is markedly earlier than that for the Ross of Mull (17.5 ± 1.0 ka) or that for Jura (16.6 ± 1.1 ka). We reject the possibility that this difference reflects nuclide inheritance in the Carn Mór samples in view of the internal consistency of the three exposure ages obtained from these sites (Fig. 10). We also reject the possibility that the summit of Carn Mór remained as a nunatak throughout the last glacial cycle as in this case the exposure ages would greatly exceed the timing of the maximum extent of the HIS, thought to be at ~27 ka or earlier (Scourse et al., 2009). Conversely, a deglaciation age of 20.6 ± 1.2 ka for Tiree is entirely consistent with offshore evidence for widespread deglaciation after ~24 ka (Scourse et al., 2009). Emergence of Carnan Mór. and the adjacent Tiree-Coll Lewisian platform probably occurred as the remnant HIS thinned during deglaciation. One possible scenario is that Tiree and the adjacent platform emerged as a nunatak that diverted southwestward ice streaming while the HIS was still operating and delivering ice onto the mid or outer shelf, implying divergent ice flow around this emerging obstruction The alignment of seafloor bedforms, however, indicates that during the period of ice streaming, ice flowed southward away from the Tiree-Coll platform to join the main trunk of the HIS south of Tiree (Fig. 3), and there is no bathymetric evidence for later divergent flow around the Tiree-Coll platform, such as overprinting of the convergent flow indicators (Fig. 3; Dove et al., 2015). As the convergent (and most recent) flowsets depicted in Fig. 3 imply ice movement southward from Tiree, it follows that deglaciation of at island at ~20.6 ± 1.2 ka approximates the timing of the cessation of ice streaming and indeed complete deglaciation across much or all of mid and outer Hebridean Shelf in this sector. This interpretation is consistent with exposure ages indicating deglaciation of the north-westernmost coast of Ireland prior to ~21 ka (Ballantyne et al., 2007; Clark et al., 2009, Table 1), as these imply widespread early deglaciation of the shelf south of the Tiree. Forthcoming radiocarbon ages also indicate that ice was absent from the mid-shelf, ~40 km southwest of Tiree, at ~21 ka supporting our interpretation (Callard et al., in prep.).

The inferred deglaciation age for the Ross of Mull (17.5 ± 1.0 ka) is significantly later than the initial deglaciation of Tiree interpreted to record the end of ice streaming at 20.6 ± 1.2 ka. The new exposure ages from Jura support the original timing of deglaciation proposed by Ballantyne et al. (2014). Combining the available

younger exposure ages we obtained from Mingulay and Barra. During this time westerly or southwesterly flow continued over Jura and Islay, and topographically confined flow (Dove et al., 2015) produced superimposed flowsets orientated NNW - SSE between Tiree and Mull (Fig. 4) with subsequent oscillatory retreat of the ice margin depositing recessional moraines (Fig. 3), here shown by red arrows. Ice margin retreat on the shelf west of Islay produces recessional moraines (red arrows) shown in Fig. 2A. Ice thinning during ongoing deglaciation leads to emergence of highest peaks on Jura and deposition of the Scriob na Caillich moraine by 16.6 ka C. By 17.5–16.5 ka widespread deglaciation has occurred across the Inner Hebrides with ice located near the present day coastline as indicated by the timing of deglaciation on Mull and Jura and exposure ages from southern Skye (Small et al., 2016) and Arran (Finlayson et al., 2014). During thinning, the ice margin became progressively topographically confined, for example within the Sound of Jura, and offshore recessional or readvance moraines, particularly in fjords indicate oscillatory retreat (Dove et al., 2015, 2016; Small et al., 2016). Bathymetry from GEBCO, onshore hillshaded DEM is derived from NASA SRTM 90 m data, available at http://www.sharegeo.ac.uk/handle/10672/5. (For interpretation of the references to colour in this figure legend, the reader is referred to the web version of this article.)

exposure ages suggests this occurred 16.6 ± 1.1 ka. Notably the exposure ages on Mull and Jura are statistically indistinguishable and in agreement with ^{36}Cl exposure ages from southern Skye which suggest ice was located near the coast at 17.6 ± 1.7 ka (Small et al., 2016) and with a basal radiocarbon age from Loch Sunart indicating deglaciation before 16.6 ± 0.3 ka (Baltzer et al., 2010). Taken together these data indicate a prolonged (~3 ka) period after initial deglaciation of Tiree and the end of ice streaming when the ice margin of the remnant HIS must have been located on the inner shelf but had not reached the present day shoreline of the Inner Hebrides.

Current empirically-based ice-sheet scale reconstructions of the retreat pattern of the BIIS (Clark et al., 2012; Hughes et al., 2016) and thermomechanical models of ice-sheet evolution (Hubbard et al., 2009) suggest that ice extended across much of the southern Hebridean shelf as late at 17–18 ka. Our new deglaciation age of 20.6 ± 1.2 ka for Tiree implies that this sector was deglaciated ~3 ka earlier. Conversely, the deglaciation ages of 17.5 ± 1.0 obtained for the Ross of Mull and 16.6 ± 1.1 for Jura are broadly consistent with the same reconstructions, which depict retreat of the ice margin to the Inner Hebrides and western mainland seaboard during the interval 16–17 ka. One implication of our results is that over the ~3 ka interval separating deglaciation of Tiree from deglaciation of southern Skye (Small et al., 2016), southern Mull and Jura, the margin of the last ice sheet in this sector underwent *net* retreat of only 50–70 km, though the presence of recessional moraines on the sea floor (Dove et al., 2015, Fig. 3) indicates that retreat was interrupted by periodic, possibly localised readvances of the ice margin. Prolonged persistence of the ice-sheet margin within a narrow corridor amongst the Inner Hebrides, as implied by our results, was anticipated by Sissons (1983) on the basis of the distribution of high coastal rock platforms that he attributed to periglacial shore erosion.

5.2. Timing of deglaciation in the outer hebrides

As outlined above, our best-estimate ages for the timing of deglaciation of Mingulay is 18.9 ± 1.0 ka, and that for northern Barra, 27 km to the north, is markedly younger (17.1 ± 1.0 ka). Less confidence can be placed on these estimates than on those for our three Inner Hebrides sites because they represent the means of only two consistent ages (cf. Small et al., 2017, Fig. 10). The only other dating evidence for the southern islands of the Outer Hebrides is a single (recalibrated) cosmogenic ^{10}Be age of 16.3 ± 0.9 ka obtained for a sample of strongly ice-moulded gneiss bedrock at 310 m on a col on South Uist, 27 km NNE of our sampling site on north Barra. Though caution is required in accepting the validity of single ages, the exposure ages from these three sites are consistent with progressive northwards deglaciation of the southernmost Outer Hebrides. At face value, our best estimate ages suggest that such deglaciation occurred slowly, with the southern margin of the Outer Hebrides Ice Cap retreating ~55 km from Mingulay to the mountains of South Uist over ~2–3 ka, but this inference must be regarded as tentative in view of the dating uncertainties associated with the Mingulay and South Uist sites.

Irrespective of the interpretation placed on the Mingulay exposure ages, however, our dates for both Mingulay and Barra indicate deglaciation ~2–3 ka after deglaciation of Tiree (20.6 ± 1.2 ka), implying that ice persisted on the southern Outer Hebrides long after the cessation of HIS ice streaming. We suggest that the most plausible explanation is that deglaciation occurred rapidly along the glacially over-deepened trough that separates the Outer Hebrides from the Tiree-Coll platform. Increased water depths and reverse bed-slopes have been shown to enhance the retreat rates of marine terminating ice streams (Jamieson et al., 2014). We suggest that accelerated calving losses in the deep trough occupied by the northern arm of the HIS resulted in rapid deglaciation of this corridor at a time when comparatively stable land-based ice occupied the southernmost islands of the Outer Hebrides. Combined with an ice divide that is inferred to have been located to the west of Barra and Mingulay (see section 3.2) this provides a mechanism by which to maintain ice cover across the southern Outer Hebrides during retreat of the ice margin in the adjacent trough, creating a marine embayment that progressively extended headward towards the southern Minch. If valid, this interpretation implies progressive severance of the southern part of the Outer Hebrides Ice Cap from the mainland ice sheet during the period ~20–17 ka, much as rapid retreat of the Minch Ice Stream progressively decoupled the northern Outer Hebrides Ice Cap from mainland ice in the North Minch (Bradwell and Stoker, 2015).

5.3. Deglaciation of the HIS

Combining the geochronological data presented here with existing geomorphological (Howe et al., 2012; Finlayson et al., 2014; Dove et al., 2015) and geochronological data (Ballantyne et al., 2007; McCabe and Clark, 2003; Clark et al., 2009; Ballantyne et al., 2014; Finlayson et al., 2014 Small et al., 2016) allows us to propose a chronologically-constrained conceptual model of the sequence of deglaciation of the southern Hebrides Shelf and the potential flow evolution of the HIS (Fig. 11). Given that the HIS drained ~10% of the former BIIS and was located close to the centre of the ice mass over the Scottish Highlands it likely had an important role in driving ice sheet dynamics during deglaciation.

Offshore IRD evidence indicates that the Hebridean sector of the BIIS underwent a major expansion towards its maximum limit at ~29 ka (Scourse et al., 2009). A distinct increase in diagnostic IRD grains in marine core MD95-2006 from the Barra-Donegal Fan has been interpreted as indicating that the ice margin reached close to the shelf edge (Knutz et al., 2001). At this time it is inferred that an ice divide straddled the North Channel, linking the Scottish and Irish ice centres, with the HIS merging with ice flowing northwest from the North Channel across the shelf (Fig. 1B; Greenwood and Clark, 2009; Dove et al., 2015). Analysis of terrestrial flowsets by Finlayson et al. (2014) suggests that subsequent development of an ice divide over the Kintyre peninsula resulted in southward flow of ice from the Firth of Clyde towards the Irish Sea Basin. This flow reorganisation appears to have diminished ice flow westward across the shelf, resulting in the HIS adopting a more southwesterly trajectory, as indicated by southwesterly orientated landforms offshore of Islay (Fig. 2A). At this time ice flowed southward off the Tiree-Coll platform, producing convergent streamlined landforms (Fig. 3). Flow was focused along two over-deepened troughs on the mid-outer shelf as indicated by streamlined landforms orientated parallel and sub-parallel to trough axes (Fig. 2B). The alignment of moraine banks on the outer shelf (Dunlop et al., 2010, Fig. 11A) suggests that they were formed by ice sourced from Scotland at a time when all of the Inner Hebrides were over-run by ice. We tentatively suggest that these moraines are related to the later period of ice streaming inferred by Dove et al. (2015), after the margin of the HIS retreated from the shelf edge. A peak in IRD delivery to the Barra-Donegal Fan apparently associated with Heinrich event H2 (Scourse et al., 2009; Hibbert et al., 2010) suggests that these moraines and the ice stream activity documented by Dove et al. (2015) may represent ice margin retreat and subsequent stabilization and flow reorganisation of the HIS in response to H2 at ~24 ka (Fig. 11A), though this inference must be regarded as tentative.

Subsequent ice thinning and retreat resulted in deglaciation of Tiree at 20.6 ± 1.2 ka, as indicated by the ^{10}Be ages presented here.

At this time the (Mingulay and Barra) were still glaciated as indicated by the fact the exposure ages from these islands post-date those from Tiree by 2–3 ka (Fig. 11B). This suggests that deglaciation north of Tiree had been focused along the northerly trough (section 5.2) with enhanced calving driven by ice margin retreat across a reverse bed-slope and into deeper waters providing a potential mechanism to account for this (cf. Jamieson et al., 2014). Similar rapid retreat may also have occurred in the trough south of Tiree, and ^{10}Be exposure ages indicate that the NW tip of Ireland was also deglaciated by this time (Ballantyne et al., 2007; Clark et al., 2009, Fig. 11B). We infer that the timing of deglaciation of Tiree marks effective cessation of the HIS, though subsequent development of localised fast flow of limited extent and duration cannot be ruled out. Superimposed flow-indicators located down-ice from the Ross of Mull (Dove et al., 2015, 2016, Fig. 4; circled in Fig. 11B) suggest the development of topographically-influenced ice flow after cessation of the HIS. The deglaciation exposure ages for Tiree and the Ross of Mull constrain this period of topographically controlled flow to the interval between 20.6 ± 1.2 ka and 17.5 ± 1.0 ka i.e. after deglaciation of Tiree but before deglaciation of the Ross of Mull (Fig. 11B–C). Associated with this period of confined flow are recessional moraines aligned perpendicular to flow direction (Figs. 2A and 3) indicate that an oscillating ice margin existed during this interval, though our deglaciation age for Jura (16.6 ± 1.1 ka) indicates that most or all of the other islands of the Inner Hebrides likely remained ice covered. Our inferred age of 18.9 ± 1.0 for Mingulay, however, suggests that the southernmost part of the Outer Hebrides Ice Cap began to retreat at ~19 ka, though as noted above this age may be maximal.

The deglaciation ages from the Ross of Mull and Jura, together with published deglaciation ages for southern Skye, Loch Sunart, and Arran (Baltzer et al., 2010; Ballantyne et al., 2014; Finlayson et al., 2014; Small et al., 2016) indicate that within the interval 17.5–16.5 ka the ice sheet margin became restricted to a corridor along the fjords, islands and peninsulas of western Scotland (Fig. 11C). Our inferred deglaciation age north Barra (17.1 ± 1.0 ka) implies northward retreat of the southern margin of the Outer Hebrides Ice Cap during the same period. Suites of offshore recessional moraines, for example SW of Skye, west of Rhum and in the Sound of Jura indicate at least local oscillations of the ice margin during overall retreat (Dove et al., 2015). The available geochronology suggests that there was widespread deglaciation across the entire ice margin of the remnant HIS from Skye in the north to Arran in the south by c. 17 ka (Fig. 11D). The progression of this deglaciation is indicated by suites of recessional moraines (e.g. Fig. 2A) in the inner marine sector of the HIS (Howe et al., 2012; Dove et al., 2015). As the high ground of Jura deglaciated the Scriob na Caillich moraine was deposited at c. 16.6 ka and ice became topographically constrained in the Sound of Jura producing southwesterly flow indicators (Fig. 8; Dove et al., 2015). In the light of the new and existing geochronological data it appears that the entire marine portion of the HIS had disappeared by~16.5 ka. The timing and style of deglaciation of the HIS is broadly similar to that inferred for the Minch Ice Stream (Fig. 1), which also involved headward recession of a calving margin and development of a marine embayment in the North Minch (Bradwell and Stoker, 2015). Cosmogenic exposure ages from a medial moraine on Skye indicate cessation of the Minch Ice Stream and an ice margin located near the present coastline by ~16.0 ka (Small et al., 2012) and the data from both ice streams are consistent with the cessation of IRD delivery to marine core MD95-2007 (Fig. 1) on the Hebridean Shelf at ~16.5 ka (Small et al., 2013).

Overall our data suggests that significant deglaciation of the marine HIS had occurred by c. 20 ka. This early deglaciation is comparable to the suggestion that the Norwegian Channel Ice Stream deglaciated at c. 22 ka (Svendsen et al., 2015) although this interpretation has been subsequently questioned (Briner et al., 2016). Within the wider BIIS initial deglaciation of the MIS from the shelf edge is inferred to have occurred at c. 28 ka (recalculated from Everest et al., 2013) while the Irish Sea Ice Stream (ISIS) did not reach its maximum until c.25.5 ka (Smedley et al., 2017) after which it underwent progressive and rapid deglaciation until c. 19 ka (Chiverrell et al., 2013). Our data do not inform directly on the timing of maximum glaciation or initial deglaciation thus it is difficult to make direct comparisons to the behaviour of these other major ice streams that drained the BIIS. It appears that maximum glaciation may have been diachronous given that initial deglaciation of the MIS occurred before the ISIS had reached its maximum extent. It would be informative to obtain direct age control on the maximum extent of the HIS to investigate if this represents a spatial (i.e, north – south) trend. Similarly the lack of dating control from the trunk of the MIS precludes making comparisons on the behaviour of the MIS *vis a vis* the HIS during the period 28–16 ka. This data gap is the subject of ongoing research of the BRITICE-CHRONO consortium however the data presented here, alongside currently available chronological constraints on the retreat of the Minch Ice Stream and the Irish Sea Ice Stream, suggest that the marine-based ice streams that drained much of the BIIS represented corridors of accelerated ice retreat flanked by more stable grounded ice masses.

6. Conclusions

New exposure ages from islands in western Scotland provide constraints on the flow evolution and deglaciation of the Hebrides Ice Stream (HIS), a major marine-based ice stream that drained the former BIIS. Thinning of the HIS at 20.6 ± 1.2 ka is recorded by exposure ages from a topographic high within the trunk of the ice stream on the island of Tiree, and this age is interpreted to constrain the cessation of large-scale regional ice streaming in this sector. Deglaciation of the northern arm of the HIS was apparently focused along submarine troughs creating a large marine embayment between the Outer and Inner Hebrides. Cosmogenic ^{10}Be exposure ages for SW Mull, Jura and the southern Outer Hebrides imply that subsequent ice retreat was much slower, and suggests that for ~3 ka an oscillating ice margin lay within a narrow corridor between Tiree and Mull. By 17.5–16.5 ka the ice margin straddled the fjords, islands and peninsulas of the western seaboard of Scotland, and the Outer Hebrides Ice Cap had shrunk to expose most of the southern Outer Hebridean islands. Our dating evidence implies much earlier retreat and cessation of the HIS than previously believed, and supports the contention that marine-termination ice streams occupying deep basins were susceptible to much more rapid retreat than adjacent grounded ice masses. This highlights the potential importance of bathymetry and calving dynamics in driving marine ice stream deglaciation, a mechanism analogous to Marine Ice Sheet Instability (Schoof, 2007).

Overall, these data provide chronological constraints on flow reorganisation of a marine-based ice stream during overall deglaciation and thus the HIS can provide a useful testing ground for high resolution numerical models, particularly at the ice stream scale, where the interaction of flow dynamics and topography becomes increasingly important.

Acknowledgements

This work was supported by the Natural Environment Research Council consortium grant; BRITICE-CHRONO (NE/J009768/1). Analysis was supported by the NERC Cosmogenic Isotope Analysis Facility allocations 9139.1013 and 9155.1014. Thanks are due to the

staff at the SUERC AMS Laboratory, East Kilbride for beryllium isotope measurements. We would like to thank Joseph Graly and an anonymous reviewer for constructive comments that have greatly improved the manuscript.

References

Alley, R.B., Clark, P.U., Huybrechts, P., Joughin, I., 2005. Ice-sheet and sea-level changes. Science 310, 456–460.

Anandakrishnan, S., Alley, R.B., Jacobel, R.W., Conway, H., 2001. Flow regime of Ice Stream C and hypotheses concerning its recent stagnation. In: Alley, R.B., Bindschadler, R.A. (Eds.), The West Antarctic Ice Sheet: Behaviour and Environment. American Geophysical Union, pp. 283–294. Antarctic Research Series, 77.

Andre, M.-F., 2002. Rates of postglacial rock weathering on glacially scoured outcrops (Abisko-Riksgransen area, 68 degrees N). Geogr. Ann. 84A, 139–150.

Andreassen, K., Laberg, J.S., Vorren, T.O., 2008. Seafloor geomorphology of the SW Barents Sea and its glaci-dynamic implications. Geomorphology 97, 157–177.

Bailey, E.B., 1924. Tertiary and Post-Tertiary Geology of Mull, Loch Aline, and Oban: a Description of Parts of Sheets 43, 44, 51, and 52 of the Geological Map, vol. 43. HMSO, Edinburgh.

Balco, G., 2011. Contributions and unrealized potential contributions of cosmogenic-nuclide exposure dating to glacier chronology, 1990–2010. Quat. Sci. Rev. 30, 3–27.

Balco, G., Stone, J.O., Lifton, N.A., Dunai, T.J., 2008. A complete and easily accessible means of calculating surface exposure ages or erosion rates from ^{10}Be and ^{26}Al measurements. Quat. Geochronol. 3, 174–195.

Balco, G., Briner, J., Finkel, R.C., Rayburn, J.A., Ridge, J.C., Schaefer, J.M., 2009. Regional beryllium-10 production rate calibration for late-glacial northeastern North America. Quat. Geochronol. 4, 93–107.

Ballantyne, C.K., 1999. Maximum altitude of late devensian glaciation on the Isle of Mull and Isle of Jura. Scott. J. Geol. 35, 97–106.

Ballantyne, C.K., Ó Cofaigh, C., 2017. The last Irish Ice Sheet: extent and chronology. In: Coxon, P., McCarron, S.G., Mitchell, F. (Eds.), Advances in Irish Quaternary Studies. Atlantis Press, Paris, pp. 101–149.

Ballantyne, C.K., McCarroll, D., Nesje, A., Dahl, S.O., Stone, J.O., 1998. The last ice sheet in north-west Scotland: reconstruction and implications. Quat. Sci. Rev. 17, 1149–1184.

Ballantyne, C.K., McCarroll, D., Stone, J.O., 2007. The Donegal ice dome, northwest Ireland: dimensions and chronology. J. Quat. Sci. 22, 773–783.

Ballantyne, C.K., Wilson, P., Gheorghiu, D., Rodés, À., 2014. Enhanced rock-slope failure following ice-sheet deglaciation: timing and causes. Earth Surf. Process. Landforms 39, 900–913.

Baltzer, A., Bates, R., Mokeddem, Z., Clet-Pellerin, M., Walter-Simonnet, A.V., Bonnot-Courtois, C., Austin, W.E., 2010. Using Seismic Facies and Pollen Analyses to Evaluate Climatically Driven Change in a Scottish Sea Loch (Fjord) over the Last 20 Ka. Geological Society, London, pp. 355–369. Special Publications, 344.

Bennett, M.R., 2003. Ice streams as the arteries of an ice sheet: their mechanics, stability and significance. Earth Sci. Rev. 61, 309–339.

Bevington, P.R., Robinson, D.K., 2003. Data Reduction and Error Analysis. McGraw-Hill.

Borchers, B., Marrero, S., Balco, G., Caffee, M., Goehring, B., Lifton, N., Nishiizumi, K., Phillips, F., Schaefer, J., Stone, J., 2016. Geological calibration of spallation production rates in the CRONUS-Earth project. Quat. Geochronol. 31, 188–198.

Bradwell, T., Stoker, M.S., 2015. Submarine sediment and landform record of a palaeo-ice stream within the British– Irish Ice Sheet. Boreas 44, 255–276.

Bradwell, T., Stoker, M.S., Golledge, N.R., Wilson, C.K., Merritt, J.W., Long, D., Everest, J.D., Hestvik, O.B., Stevenson, A.G., Hubbard, A.L., Finlayson, A.G., 2008. The northern sector of the last British Ice Sheet: maximum extent and demise. Earth Sci. Rev. 88, 207–226.

Bronk Ramsey, C., 2013. OxCal 4.2. Manual [online] available at. http://c14.arch.ox.ac.uk/oxcalhelp/hlp_contents.html.

Briner, J.P., Bini, A.C., Anderson, R.S., 2009. Rapid early Holocene retreat of a Laurentide outlet glacier through an Arctic fjord. Nat. Geosci. 2, 496–499.

Briner, J.P., Goehring, B.M., Mangerud, J., Svendsen, J.I., 2016. The deep accumulation of ^{10}Be at Utsira, southwestern Norway: implications for cosmogenic nuclide exposure dating in peripheral ice sheet landscapes. Geophys. Res. Lett. 43, 9121–9129.

Catania, G.A., Scambos, T.A., Conway, H., Raymond, C.F., 2006. Sequential stagnation of Kamb ice stream, West Antarctica. Geophys. Res. Lett. 33, L14502.

Clark, C.D., 1997. Reconstructing the evolutionary dynamics of former ice sheets using multi-temporal evidence, remote sensing and GIS. Quat. Sci. Rev. 16, 1067–1092.

Clark, C.D., Hughes, A.L., Greenwood, S.L., Jordan, C., Sejrup, H.P., 2012. Pattern and timing of retreat of the last British-Irish ice sheet. Quat. Sci. Rev. 44, 112–146.

Clark, J., McCabe, A., Schnabel, C., Clark, P.U., Freeman, S., Maden, C., Xu, S., 2009. ^{10}Be chronology of the last deglaciation of County Donegal, northwestern Ireland. Boreas 38, 111–118.

Child, D., Elliott, G., Mifsud, C., Smith, A.M., Fink, D., 2000. Sample processing for earth science studies at ANTARES. Nucl. Instrum. Methods Phys. Res. Sect. B Beam Interact. Mater. Atoms 172 (1), 856–860.

Chiverrell, R.C., Thrasher, I.M., Thomas, G.S., Lang, A., Scourse, J.D., van Landeghem, K.J., McCarroll, D., Clark, C.D., Cofaigh, C.Ó., Evans, D.J., Ballantyne, C.K., 2013. Bayesian modelling the retreat of the Irish sea ice stream. J. Quat. Sci. 28, 200–209.

Conway, H., Catania, G., Raymond, C.F., Gades, A.M., Scambos, T.A., Engelhardt, H., 2002. Switch of flow direction in an Antarctic ice stream. Nature 419, 465–467.

Dawson, A.G., 1979. A Devensian medial moraine in Jura. Scott. J. Geol. 15, 43–48.

Dawson, A.G., 1982. Lateglacial sea-level changes and ice-limits in Islay, Jura and Scarba, Scottish inner Hebrides. Scott. J. Geol. 18, 253–265.

Dawson, A.G., 1994. Strandflat development and Quaternary shorelines on Tiree and Coll, Scottish Hebrides. J. Quat. Sci. 9, 349–356.

De Angelis, H., Kleman, J., 2007. Palaeo-ice streams in the Foxe/Baffin sector of the Laurentide ice sheet. Quat. Sci. Rev. 26, 1313–1331.

DeConto, R.M., Pollard, D., 2016. Contribution of Antarctica to past and future sea-level rise. Nature 531, 591–597.

Dove, D., Arosio, R., Finlayson, A., Bradwell, T., Howe, J.A., 2015. Submarine glacial landforms record late Pleistocene ice-sheet dynamics, inner Hebrides, Scotland. Quat. Sci. Rev. 123, 76–90.

Dove, D., Finlayson, A., Bradwell, T., Howe, J.A., Arosio, R., 2016. Deglacial Landform Assemblage Records Fast Ice-flow and Retreat, Inner Hebrides, Scotland. Geological Society, London, pp. 135–138. Memoirs, 46.

Dunlop, P., Shannon, R., McCabe, M., Quinn, R., Doyle, E., 2010. Marine geophysical evidence for ice sheet extension and recession on the Malin Shelf: new evidence for the western limits of the British Irish Ice Sheet. Mar. Geol. 276, 86–99.

Dyke, A.S., Morris, T.F., 1988. Drumlin fields, dispersal trains, and ice streams in Arctic Canada. Can. Geogr. 32, 86–90.

Everest, J.D., Bradwell, T., Stoker, M., Dewey, S., 2013. New age constraints for the maximum extent of the last British–Irish Ice Sheet (NW sector). J. Quat. Sci. 28 (1), 2–7.

Favier, L., Durand, G., Cornford, S.L., Gudmundsson, G.H., Gagliardini, O., Gillet-Chaulet, F., Zwinger, T., Payne, A.J., Le Brocq, A.M., 2014. Retreat of Pine Island Glacier controlled by marine ice-sheet instability. Nat. Clim. Change 4, 117–121.

Fabel, D., Ballantyne, C.K., Xu, S., 2012. Trimlines, blockfields, mountain-top erratics and the vertical dimensions of the last British–Irish Ice Sheet in NW Scotland. Quat. Sci. Rev. 55, 91–102.

Fenton, C.R., Hermanns, R.L., Blikra, L.H., Kubik, P.W., Bryant, C., Niedermann, S., Meixner, A., Goethals, M.M., 2011. Regional ^{10}Be production rate calibration for the past 12 ka deduced from the radiocarbon-dated Grøtlandsura and Russenes rock avalanches at 69 N, Norway. Quat. Geochronol. 6, 437–452.

Finlayson, A., Fabel, D., Bradwell, T., Sugden, D., 2014. Growth and decay of a marine terminating sector of the last British–Irish Ice Sheet: a geomorphological reconstruction. Quat. Sci. Rev. 83, 28–45.

Flinn, D., 1978. The glaciation of the outer Hebrides. Geol. J. 13, 195–199.

Goehring, B.M., Lohne, Ø.S., Mangerud, J., Svendsen, J.I., Gyllencreutz, R., Schaefer, J., Finkel, R., 2012. Late glacial and Holocene ^{10}Be production rates for western Norway. J. Quat. Sci. 27, 89–96.

Greenwood, S.L., Clark, C.D., 2009. Reconstructing the last Irish Ice Sheet 1: changing flow geometries and ice flow dynamics deciphered from the glacial landform record. Quat. Sci. Rev. 28, 3085–3100.

Harker, A., 1901. Ice erosion in the Cuillin hills, Skye. Trans. R. Soc. Edinb. 40, 221–252.

Heyman, J., Stroeven, A.P., Harbor, J.M., Caffee, M.W., 2011. Too young or too old: evaluating cosmogenic exposure dating based on an analysis of compiled boulder exposure ages. Earth Planet. Sci. Lett. 302, 71–80.

Hibbert, F.D., Austin, W.E., Leng, M.J., Gatliff, R.W., 2010. British Ice Sheet dynamics inferred from North Atlantic ice-rafted debris records spanning the last 175 000 years. J. Quat. Sci. 25, 461–482.

Hiemstra, J.F., Shakesby, R.A., Vieli, A., 2013. Late Quaternary glaciation in the Hebrides sector of the continental shelf: was St Kilda overrun by the British-Irish ice sheet? Boreas 44, 178–196.

Howat, I.M., Joughin, I., Scambos, T.A., 2007. Rapid changes in ice discharge from Greenland outlet glaciers. Science 315, 1559–1561.

Howe, J.A., Dove, D., Bradwell, T., Gafeira, J., 2012. Submarine geomorphology and glacial history of the Sea of the Hebrides, UK. Mar. Geol. 315, 64–76.

Hubbard, A., Bradwell, T., Golledge, N., Hall, A., Patton, H., Sugden, D., Cooper, R., Stoker, M., 2009. Dynamic cycles, ice streams and their impact on the extent, chronology and deglaciation of the British–Irish ice sheet. Quat. Sci. Rev. 28, 758–776.

Hughes, A.L.C., Clark, C.D., Jordan, C.J., 2014. Flow-pattern evolution of the last British ice sheet. Quat. Sci. Rev. 89, 148–168.

Hughes, A.L., Gyllencreutz, R., Lohne, Ø.S., Mangerud, J., Svendsen, J.I., 2016. The last Eurasian ice sheets–a chronological database and time-slice reconstruction, DATED-1. Boreas 45, 1–45.

Hulbe, C.L., Fahnestock, M.A., 2004. West Antarctic ice-stream discharge variability: mechanism, controls and pattern of grounding-line retreat. J. Glaciol. 50, 471–484.

Jacobel, R.W., Scambos, T.A., Raymond, C.F., Gades, A.M., 1996. Changes in the configuration of ice stream flow from the West Antarctic ice sheet. J. Geophys. Res. Solid Earth 101, 5499–5504.

Jamieson, S.S., Vieli, A., Cofaigh, C.Ó., Stokes, C.R., Livingstone, S.J., Hillenbrand, C.D., 2014. Understanding controls on rapid ice-stream retreat during the last deglaciation of Marguerite Bay, Antarctica, using a numerical model. J. Geophys. Res. Earth Surf. 119, 247–263.

Joughin, I., Abdalati, W., Fahnestock, M., 2004. Large fluctuations in speed on Greenland's Jakobshavn Isbrae glacier. Nature 432, 608–610.

Kaplan, M.R., Strelin, J.A., Schaefer, J.M., Denton, G.H., Finkel, R.C., Schwartz, R., Putnam, A.E., Vandergoes, M.J., Goehring, B.M., Travis, S.G., 2011. In-situ

cosmogenic ^{10}Be production rate at Lago Argentino, Patagonia: implications for late-glacial climate chronology. Earth Planet. Sci. Lett. 309, 21–32.
Kleman, J., Hättestrand, C., Stroeven, A.P., Jansson, K.N., De Angelis, H., Borgström, I., 2006. Reconstruction of palaeo-ice sheets-inversion of their glacial geomorphological record. In: Knight, P.G. (Ed.), Glacier Science and Environmental Change. Blackwell Publishing, Malden, MA, USA, pp. 192–198.
Knutz, P.C., Austin, W.E., Jones, E.J.W., 2001. Millennial-scale depositional cycles related to British ice sheet variability and north Atlantic paleocirculation since 45 kyr BP, Barra Fan, UK margin. Paleoceanography 16, 53–64.
Kohl, C.P., Nishiizumi, K., 1992. Chemical isolation of quartz for measurement of in-situ-produced cosmogenic nuclides. Geochim. Cosmochim. Acta 56, 3583–3587.
Lal, D., 1991. Cosmic ray labeling of erosion surfaces: in situ nuclide production rates and erosion models. Earth Planet. Sci. Lett. 104, 424–439.
Lane, T.P., Roberts, D.H., Rea, B.R., Cofaigh, C.Ó., Vieli, A., Rodés, A., 2014. Controls upon the Last Glacial maximum deglaciation of the northern Uummannaq ice stream system, West Greenland. Quat. Sci. Rev. 92, 324–344.
Lifton, N., Sato, T., Dunai, T.J., 2014. Scaling in situ cosmogenic nuclide production rates using analytical approximations to atmospheric cosmic-ray fluxes. Earth Planet. Sci. Lett. 386, 149–160.
MacLeod, A., Palmer, A., Lowe, J., Rose, J., Bryant, C., Merritt, J., 2011. Timing of glacier response to Younger Dryas climatic cooling in Scotland. Glob. Planet. Change 79, 264–274.
MacLeod, A., Matthews, I.P., Lowe, J.J., Palmer, A.P., Albert, P.G., 2015. A second tephra isochron for the Younger Dryas period in northern Europe: the Abernethy Tephra. Quat. Geochronol. 28, 1–11.
Margold, M., Stokes, C.R., Clark, C.D., 2015. Ice streams in the Laurentide Ice Sheet: identification, characteristics and comparison to modern ice sheets. Earth Sci. Rev. 143, 117–146.
Marrero, S.M., Phillips, F.M., Borchers, B., Lifton, N., Aumer, R., Balco, G., 2016. Cosmogenic nuclide systematics and the CRONUScalc program. Quat. Geochronol. 31, 160–187.
McCabe, A.M., Clark, P.U., 2003. Deglacial chronology from County Donegal, Ireland: implications for deglaciation of the British–Irish ice sheet. J. Geol. Soc. 160, 847–855.
Ó'Cofaigh, C., Evans, D.J., 2001. Deforming bed conditions associated with a major ice stream of the last British ice sheet. Geology 29, 795–798.
Ó'Cofaigh, C., Dowdeswell, J.A., Allen, C.S., Hiemstra, J.F., Pudsey, C.J., Evans, J., Evans, D.J., 2005. Flow dynamics and till genesis associated with a marine-based Antarctic palaeo-ice stream. Quat. Sci. Rev. 24, 709–740.
Ottesen, D., Dowdeswell, J.A., Rise, L., 2005. Submarine landforms and the reconstruction of fast-flowing ice streams within a large Quaternary ice sheet: the 2500-km-long Norwegian-Svalbard margin (57–80° N). Geol. Soc. Am. Bull. 117, 1033–1050.
Patton, H., Hubbard, A., Andreassen, K., Winsborrow, M., Stroeven, A.P., 2016. The build-up, configuration, and dynamical sensitivity of the Eurasian ice-sheet complex to Late Weichselian climatic and oceanic forcing. Quat. Sci. Rev. 153, 97–121.
Payne, A.J., Vieli, A., Shepherd, A.P., Wingham, D.J., Rignot, E., 2004. Recent dramatic thinning of largest West Antarctic ice stream triggered by oceans. Geophys. Res. Lett. 31 (23).
Peacock, J.D., 1981. Quaternary research association excursion guide: Lewis and Harris. Quat. Newsl. 35, 45–54.
Peacock, J.D., 1984. Quaternary Geology of the Outer Hebrides. British Geological Survey Reports, no. 16/2.
Peacock, J.D., 1991. Glacial deposits of the Hebridean region. In: Ehlers, J., Gibbard, P.L., Rose, J. (Eds.), Glacial Deposits of Great Britain and Ireland. Balkema, Rotterdam, pp. 109–119.
Peacock, J.D., 2008. Late Devensian palaeoenvironmental changes in the sea area adjacent to Islay, SW Scotland: implications for the deglacial history of the island. Scott. J. Geol. 44, 183–190.
Putnam, A.E., Schaefer, J.M., Barrell, D.J.A., Vandergoes, M., Denton, G.H., Kaplan, M.R., Finkel, R.C., Schwartz, R., Goehring, B.M., Kelley, S.E., 2010. In situ cosmogenic ^{10}Be production-rate calibration from the Southern Alps, New Zealand. Quat. Geochronol. 5, 392–409.
Reimer, P.J., Bard, E., Bayliss, A., Beck, J.W., Blackwell, P.G., Bronk Ramsey, C., Buck, C.E., Cheng, H., Edwards, R.L., Friedrich, M., Grootes, P.M., 2013. IntCal13 and Marine13 radiocarbon age calibration curves 0–50,000 years cal BP. Radiocarbon 55, 1869–1887.
Retzlaff, R., Bentley, C.R., 1993. Timing of stagnation of Ice Stream C, West Antarctica, from short-pulse radar studies of buried surface crevasses. J. Glaciol. 39, 553–561.
Roberts, D.H., Long, A.J., Davies, B.J., Simpson, M.J., Schnabel, C., 2010. Ice stream influence on west Greenland ice sheet dynamics during the last glacial maximum. J. Quat. Sci. 25, 850–864.
Roberts, D.H., Rea, B.R., Lane, T.P., Schnabel, C., Rodés, A., 2013. New constraints on Greenland ice sheet dynamics during the last glacial cycle: evidence from the Uummannaq ice stream system. J. Geophys. Res. Earth Surf. 118, 519–541.
Schoof, C., 2007. Ice sheet grounding line dynamics: Steady states, stability, and hysteresis. J. Geophys. Res. Earth Surf. 112, F03S28.
Scourse, J.D., Haapaniemi, A.I., Colmenero-Hidalgo, E., Peck, V.L., Hall, I.R., Austin, W.E., Knutz, P.C., Zahn, R., 2009. Growth, dynamics and deglaciation of the last British–Irish ice sheet: the deep-sea ice-rafted detritus record. Quat. Sci. Rev. 28, 3066–3084.
Sejrup, H.P., Larsen, E., Haflidason, H., Berstad, I.M., Hjelstuen, B.O., Jonsdottir, H.E., King, E.L., Landvik, J., Longva, O., Nygård, A., Ottesen, D., 2003. Configuration, history and impact of the Norwegian Channel ice stream. Boreas 32, 18–36.
Shepherd, A., Wingham, D., Rignot, E., 2004. Warm ocean is eroding West Antarctic ice sheet. Geophys. Res. Lett. 31, L23402.
Sissons, J.B., 1981. The last Scottish ice-sheet: facts and speculative discussion. Boreas 10, 1–17.
Sissons, J.B., 1983. The Quaternary geomorphology of the Inner Hebrides: a review and reassessment. Proc. Geol. Assoc. 94, 165–175.
Small, D., Fabel, D., 2015. A Lateglacial ^{10}Be production rate from glacial lake shorelines in Scotland. J. Quat. Sci. 30, 509–513.
Small, D., Rinterknecht, V., Austin, W., Fabel, D., Miguens-Rodriguez, M., 2012. In situ cosmogenic exposure ages from the Isle of Skye, northwest Scotland: implications for the timing of deglaciation and readvance from 15 to 11 ka. J. Quat. Sci. 27, 150–158.
Small, D., Austin, W., Rinterknecht, V., 2013. Freshwater influx, hydrographic reorganization and the dispersal of ice-rafted detritus in the sub-polar North Atlantic Ocean during the last deglaciation. J. Quat. Sci. 28, 527–535.
Small, D., Rinterknecht, V., Austin, W.E.N., Bates, C.R., Benn, D.I., Scourse, J.D., Bourlès, D.L., ASTER Team, Hibbert, F.D., 2016. Implications of ^{36}Cl exposure ages from Skye, northwest Scotland for the timing of ice stream deglaciation and deglacial ice dynamics. Quat. Sci. Rev. 150, 130–145.
Small, D., Clark, C.D., Chiverrell, R.C., Smedley, R.K., Bateman, M.D., Duller, G.A.T., Ely, J.C., Fabel, D., Medialdea, A., Moreton, S.G., 2017. Devising quality assurance procedures for assessment of legacy geochronological data relating to deglaciation of the last British-Irish Ice Sheet. Earth Sci. Rev. 164, 232–250.
Smedley, R.K., Scourse, J.D., Small, D., Hiemstra, J.F., Duller, G.A.T., Bateman, M.D., Burke, M.J., Chiverrell, R.C., Clark, C.D., Davies, S.M., Fabel, D., 2017. New age constraints for the limit of the British–Irish ice sheet on the Isles of Scilly. J. Quat. Sci. 32, 48–62.
Stoker, M., Bradwell, T., 2005. The Minch palaeo-ice stream, NW sector of the British–Irish ice sheet. J. Geol. Soc. 162, 425–428.
Stokes, C.R., Clark, C.D., 2001. Palaeo-ice streams. Quat. Sci. Rev. 20, 1437–1457.
Stokes, C.R., Clark, C.D., Darby, D.A., Hodgson, D.A., 2005. Late Pleistocene ice export events into the Arctic ocean from the M'Clure strait ice stream, Canadian Arctic Archipelago. Glob. Planet. Change 49, 139–162.
Stokes, C.R., Clark, C.D., Storrar, R., 2009. Major changes in ice stream dynamics during deglaciation of the north-western margin of the Laurentide Ice Sheet. Quat. Sci. Rev. 28, 721–738.
Stokes, C.R., Margold, M., Clark, C.D., Tarasov, L., 2016. Ice stream activity scaled to ice sheet volume during Laurentide Ice Sheet deglaciation. Nature 530, 322–326.
Stone, J.O., 2000. Air pressure and cosmogenic isotope production. J. Geophys. Res. Solid Earth 105, 23753–23759.
Stone, J.O., Ballantyne, C.K., 2006. Dimensions and deglacial chronology of the Outer Hebrides Ice Cap, northwest Scotland: implications of cosmic ray exposure dating. J. Quat. Sci. 21, 75–84.
Svendsen, J.I., Briner, J.P., Mangerud, J., Young, N.E., 2015. Early break-up of the Norwegian Channel ice stream during the last glacial maximum. Quat. Sci. Rev. 107, 231–242.
Synge, F.M., Stephens, N., 1966. Late-and post-glacial shorelines, and ice limits in Argyll and north-east Ulster. Trans. Inst. Br. Geogr. 39, 101–125.
Von Weymarn, J.A., 1979. A new concept of glaciation in Lewis and Harris, outer Hebrides. Proceedings of the Royal Society of Edinburgh. Section B. Biol. Sci. 77, 97–105.
Winsborrow, M.C., Stokes, C.R., Andreassen, K., 2012. Ice-stream flow switching during deglaciation of the southwestern Barents Sea. Geol. Soc. Am. Bull. 124, 275–290.
Xu, S., Dougans, A.B., Freeman, S.P., Schnabel, C., Wilcken, K.M., 2010. Improved ^{10}Be and ^{26}Al-AMS with a 5MV spectrometer. Nucl. Instrum. Methods Phys. Res. Sect. B Beam Interact. Mater. Atoms 268, 736–738.
Young, N.E., Schaefer, J.M., Briner, J.P., Goehring, B.M., 2013. A ^{10}Be production-rate calibration for the Arctic. J. Quat. Sci. 28, 515–526.